Society for Mathematical Biology

CrossMark

Computational Approaches and Analysis for a Spatio-Structural-Temporal Invasive Carcinoma Model

Arran Hodgkinson[1] · Mark A. J. Chaplain[2] ·
Pia Domschke[3] · Dumitru Trucu[4]

Abstract Spatio-temporal models have long been used to describe biological systems of cancer, but it has not been until very recently that increased attention has been paid to structural dynamics of the interaction between cancer populations and the molecular mechanisms associated with local invasion. One system that is of particular interest is that of the urokinase plasminogen activator (uPA) wherein uPA binds uPA receptors on the cancer cell surface, allowing plasminogen to be cleaved into plasmin, which degrades the extracellular matrix and this way leads to enhanced cancer cell migration. In this paper, we develop a novel numerical approach and associated analysis for spatio-structuro-temporal modelling of the uPA system for up to two-spatial and two-structural dimensions. This is accompanied by analytical exploration of the numerical techniques used in simulating this system, with special consideration being given to the proof of stability within numerical regimes encapsulating a central differences approach to approximating numerical gradients. The stability analysis performed here

✉ Dumitru Trucu
  trucu@maths.dundee.ac.uk

  Arran Hodgkinson
  arran.hodgkinson@umontpellier.fr

  Mark A. J. Chaplain
  majc@st-andrews.ac.uk

  Pia Domschke
  domschke@mathematik.tu-darmstadt.de

[1] DIMNP, Université de Montpellier II, 34095 Montpellier, France

[2] School of Mathematics and Statistics, Mathematical Institute, University of St. Andrews, St. Andrews, Scotland KY16 9SS, UK

[3] Fachbereich Mathematik, Technische Universität Darmstadt, 64293 Darmstadt, Germany

[4] Division of Mathematics, University of Dundee, Dundee, Scotland DD1 4HN, UK

reveals instabilities induced by the coupling of the structural binding and proliferative processes. The numerical results expound how the uPA system aids the tumour in invading the local stroma, whilst the inhibitor to this system may impede this behaviour and encourage a more sporadic pattern of invasion.

Keywords Cancer invasion · Structured cell population dynamics · Computational modelling

Mathematics Subject Classification 22E46 · 53C35 · 57S20

1 Introduction

Over the past three decades or so, the processes involved in cancer growth and spread received significant mathematical attention through novel and increasingly sophisticated modelling approaches (Prigogine and Lefever 1980; Meinzer and Sandblad 1985; Murray and Oster 1984; Anderson et al. 2000; Galle et al. 2009), leading to a deeper understanding of key cancer development aspects with potential therapeutic importance (Dufau et al. 2012; Benzekry et al. 2014).

While being sometimes regarded as a paradigm of local tissue remodelling, cancer invasion is a crucially important process in the overall cancer development where complex heterotypic cell population processes combined with a cascade of molecular signalling mechanisms lead to the degradation the healthy tissue and its concomitant repopulation by migratory cancer cells (Danø and Rømer 1999; Hanahan and Weinberg 2011). This attracted a wide range of spatio-temporal modelling at either one spatial scale (Anderson et al. 2000; Gatenby and Gawlinski 1996; Anderson and Chaplain 1998; Chaplain et al. 2001; Chaplain and Lolas 2005) or in a multiscale approach (Trucu et al. 2013; Peng et al. 2017). It became increasingly apparent, however, that the context of macro-scale spatio-temporal modelling was not sufficient to take into account the intricate behaviour of cancer cell processes. To that end, with insights from important concepts in structural modelling of biological systems (considering age, size, etc.) (Diekmann et al. 1984; Kunisch et al. 1985; Metz and Diekmann 1986; Clayton and Schifflers 1987; Diekmann and Metz 1994; Basse and Ubezio 2007), the various spatio-temporal modelling approaches for cancer invasion have been recently complemented by structural models (Chapman et al. 2007; Domschke et al. 2017), which enable a more detailed description of the involved biological processes by implicitly accounting for a certain extent of single cell-dynamics.

One biological system, important in cancer invasion, that has received increased attention in recent years has been termed the urokinase plasminogen activator (uPA) system (Peng et al. 2017; Smith and Marshall 2010; Persson et al. 2012). The uPA protein has long been noted as a marker of various cancer types, such as colorectal, gastric, oesophageal, lung, cervical, ovarian, renal, pancreatic, and hepatocellular, with its greatest prognostic evidence being derived from strains of breast cancer (Duffy et al. 1999). The reduction in uPA expression in peritumoural tissue also causes this protein to be of great clinical significance, such that expression remains localised to the cancerous tissue (Bhuvarahamurthy et al. 2005; Li and Cozzi 2007).

Urokinase plasminogen activator receptor (uPAR) is a protein anchored to the cell surface and, bound with high affinity to uPA (Sugioka et al. 2013), aids the degradation of the extracellular matrix (ECM) (Kondraganti et al. 2006; Liang et al. 2008). X-ray analysis of the uPA–uPAR complex has revealed that uPA binds its receptor on a subsurface encapsulated by all three of its major interactive domains (Huai et al. 2006; Barinka et al. 2006). Neither uPAR nor unbound uPA is intrinsically active within the human tissue due to their folding being unfavourable to binding plasminogen, until formation of the uPA–uPAR complex (Ellis and Danø 1993). Regardless of the biological paradigm, however, uPA retains its high specificity for plasminogen (Rijken 1995).

Further to this, the binding structure of these proteins allows the binding regions of the uPAR protein to become available for plasminogen protein interactions. The ability of the cell to advantageously manipulate its environment and achieve local dominance is further altered by this chemical adaptation. This process is mediated through changes to cellular capabilities when bound to activated uPA–uPAR complexes, enabling greater survival, adhesion, and migration (Binder et al. 2007). It has been shown that even modest increases in the presence of this surface bound complex are sufficient to greatly increase the prolific and proteolytic activities of invasive tumour cells (Stillfried et al. 2007). Moreover, bound uPA is susceptible to being further bound by the class of inhibitory proteins referred to as uPA inhibitor-1 (PAI-1).

The cancer invasive process is further augmented through integrin-mediated signalling pathways utilised by the uPA–uPAR complex (Khanna et al. 2011). Perhaps most significant is the activation of the protein class known as $\alpha 5\beta 1$ integrin, which actively recruits the epidermal growth factor receptor (EGFR), an upstream signalling protein whose presence has been an indicator for high levels of extracellular signal-regulated kinases (ERKs) (Liu et al. 2002). As an essential upregulator of mitotic activity in cancerous cells, ERKs enhance the proteolytic dynamics of the cancer cell population (Chaurasia et al. 2006).

Furthermore, the complex formed between uPA and uPAR also increases the avidity of uPAR for vitronectin, an important protein for cell-ECM adhesion (Waltz et al. 1997). Vitronectin is a protein found primarily within plasma or deposited within the ECM, where it weakly binds the intra-matrix vitronectin receptor (Wei et al. 1994). The unbound receptor, uPAR, will further selectively bind vitronectin and increase cellular adhesion to the ECM (Waltz and Chapman 1994), whereas bound uPAR is an exceptionally high affinity receptor for vitronectin (Wei et al. 1994; Waltz and Chapman 1994).

Cancer cell migration is enhanced through the downstream synthesis of matrix metalloproteinases (MMPs), after the activation of conformal pro-MMP proteins by locally activated plasminogen, which degrade the ECM and enable local tumour invasion (Danø and Rømer 1999). The growth of the tumour, however, then activates a negative feedback loop through the downstream upregulation of PAI-1 synthesis (Godár et al. 1999; Leksa et al. 2002).

There is significant evidence that proteolytic enzymes (which degrade the collagen of the ECM) can be activated by an increased presence of activated plasminogen (Madsen et al. 2007; Danø et al. 1985). Primarily, the function of uPA is the conversion of plasminogen to plasmin; known to be a key regulator of these proteolytic proteins

(Danø et al. 1985). In this context, matrix metalloproteinase 2 (MMP2) is a major target for plasmin, causing increased degradation of the ECM and incorporation of the degraded collagen into localised plaques (Peng et al. 2006; Madsen et al. 2007).

Finally, a specifically prolific feature of the the uPA–uPAR complex (in relation to its environment) is that in its active conversion of plasminogen to plasmin it encourages the production of the proenzyme single-chain urokinase plasminogen activator (scuPA). This scuPA protein is the precursor of uPA and therefore closes a positive feedback loop which is integral to the success of cancer cells in their invasive pursuit (Binder et al. 2007). Plasmin is also capable of activating scuPA by cleaving a bond named Lys158 (Rijken 1995), contributing to the feedback mechanism. There is mounting evidence that the majority of these feedback mechanisms are localised to the tumour's invading edge (Waltz et al. 1997; Danø and Rømer 1999).

Based upon the biological evidence discussed so far, it is therefore crucially important to account for the molecular binding of the uPA components in modelling cancer dynamics. To that end, the general modelling approach introduced in Domschke et al. (2017), where a novel spatio-temporal-structural model was derived for a general tissue dynamics involving cells, ECM, and several accompanying populations of potentially membrane binding molecules, therefore offers an appropriate framework.

The model proposed by Domschke et al. (2017) is a recent advancement within the well established area of a structured population modelling, uniquely utilising the structural dynamics to describe spatio-chemical-temporal processes in the tumour cell population. With a history stretching over almost six decades, however, structured population models address a whole range of research challenges arising across many biomedical and ecological areas, including epidemiology, collective movement either within cell population (such as those in cancer invasion or embryogenesis) or within social crowd dynamics. Varying in scope and purpose, these range from temporal–structural approaches (where space is ignored, and time is coupled for instance with "age" or "size" structure) (Trucco 1965a, b; Sinko and Streifer 1967; Gyllenberg 1982; Diekmann et al. 1984; Kunisch et al. 1985; Gyllenberg 1986; Gyllenberg and Webb 1987; Tucker and Zimmerman 1988; Diekmann et al. 1992; Diekmann and Metz 1994; Huyer 1994; Calsina and Saldaña 1995; de Roos 1997; Cushing 1998; Basse and Ubezio 2007; Chapman et al. 2007), to spatio-structural models (where time is ignored) (Gurtin and MacCamy 1981; MacCamy 1981; Diekmann and Temme 1982; Garroni and Langlais 1982; Huang 1994; Rhandi 1998; Langlais 1988; Langlais and Milner 2003; Ayati 2006; Delgado et al. 2006; Allen 2009), and finally to more complex approaches that couple time, space, and structure (Di Blasio 1979; Busenberg and Iannelli 1983; Langlais 1988; Fitzgibbon et al. 1995; So et al. 2001; Al-Omari and Gourley 2002; Cusulin et al. 2005; Deng and Hallam 2006; Domschke et al. 2017; Trucu et al. 2017). Specifically, important examples of structured approaches in cancer modelling include size-structured models (Gyilenberg and Webb 1990) (which account for cell size in order to understand cell cycle dynamics), age-structured models (Bertuzzi et al. 2004; Dyson and Webb 2000a, b) (which account for the age distribution of the population), as well as more specific models taking into account various other aspects such as RNA content (Kimmel et al. 1984), mutational state (Delitala and Lorenzi 2012; Lorz et al. 2013; Delitala et al. 2015), popular altruism (Hsieh 1991) and more. For a more extensive introduction to and analysis of these structured cancer

development models, one may refer to the review papers by Bellomo and Preziosi (2000), Bellomo et al. (2008) as well as to a number of relevant books on this topic (Adam and Bellomo 1996; Cushing 1998; Perthame 2007; Magal and Ruan 2008).

Thus, adopting here the notations from Domschke et al. (2017), in this paper we propose appropriate computational approaches and resulting simulation alongside associated analysis to explore the spatio-temporal-structural modelling of a cancerous tissue consisting of:

– a structured cancer cell density $c(t, x, y)$, with $(t, x, y) \in \mathcal{I} \times \mathcal{D} \times \mathcal{P}$, where $\mathcal{I} := [0, T]$ is a time interval, $\mathcal{D} \in \mathbb{R}^d$, $d = 1, 2$, is the spatial tumour domain, and $\mathcal{P} \subset \mathbb{R}^p$ is a cone of appropriate dimension $p \leq 2$ representing the set of all admissible membrane binding structures for the uPA system;
– ECM density $v(t, x)$, with $(t, x) \in \mathcal{I} \times \mathcal{D}$;
– $q \leq 3$ components of the uPA system (uPA, PAI-1, and plasmin), which are appropriately grouped in binding and unbinding classes of molecular species represented here by $m_b := [m_{b,1}(t, x), \ldots, m_{b,p}(t, x)]^{\mathrm{T}} \in \mathbb{R}^p$ and $m_f := [m_{f,1}(t, x), \ldots, m_{f,q-p}(t, x)]^{\mathrm{T}} \in \mathbb{R}^{q-p}$, respectively.

2 Structured Model for Cancer Modelling Exploring the uPA Binding Dynamics

Using the theoretical framework derived in Domschke et al. (2017), we explore the dynamics of a cancerous tissue of the resulting spatio-temporal-structural uPA modelling system, which we briefly describe here as follows. Per unit time, under the presence of a cell proliferation law, we generally assume that the spatial dynamics of the cancer cell population is dictated by diffusion, chemotaxis, haptotaxis, and cell-adhesion. The molecular binding and unbinding of the uPA components (uPA or PAI-1) are accounted for in this framework (Domschke et al. 2017) in terms of an appropriately derived structural cone $\mathcal{P}$ (detailed on specific cases in the following sections), and the resulting dynamics leads not only to a spatio-temporal migration but also to a structural evolution of the cancer population $c(t, x, y)$. The influence of cell-adhesion over the spatial dynamics at x is considered here in non-structured fashion and, similar to other previous approaches (Domschke et al. 2014; Gerisch and Chaplain 2008), this is captured via a non-local term that represents the cell-cell and cell matrix adhesion interactions within a sensing region of radius R. This non-local term is of the form

$$\mathcal{A}(t, x, y, \mathbf{u}(t, \cdot)) = \frac{1}{R} \int\limits_{B(0,R)} \mathbf{n}(\tilde{x}) \mathcal{K}(\| \tilde{x} \|_2) g(t, y, \mathbf{u}(t, x + \tilde{x})) \chi_{\mathcal{D}}(x + \tilde{x}) \, d\tilde{x} \quad (1)$$

where, for any $\tilde{x} \in B(0, R)$, $\mathbf{n}(\tilde{x})$ represents the unit vector pointing from x to $x + \tilde{x}$, $\mathcal{K}(\cdot)$ is a smooth spatial kernel, and the adhesion function $g(t, y, \mathbf{u}(t, x + \tilde{x}))$ accounts for the cell-cell and cell-matrix adhesion strengths S_{cc} and S_{cv}, respectively, this being given by

$$g(t, y, \mathbf{u}) = \left[S_{cc}(t) \int\limits_{\mathcal{P}} c \, dy + S_{cv}(t) v \right] \cdot (1 - \rho(\mathbf{u}))^+, \quad (2)$$

with the convenient vector notation

$$\mathbf{u}(t, x) := \left[\int_{\mathcal{P}} c(t, x, y) \mathrm{d}y, \ v(t, x) \right]^{\mathrm{T}}$$

and $(\cdot)^+ := \max\{0, \cdot\}$. Furthermore, as the ECM density $v(t, x)$ is only diminished and remodelled by the cancer cells and that the unbound (free) part of the considered components of the uPA system that are produced by the cancer cells are only diffusing in the tumour domain, the structured system that is obtained via the general modelling framework from Domschke et al. (2017) is as follows:

$$
\begin{cases}
\frac{\partial c}{\partial t} = \nabla_x \cdot \left[D_c \nabla_x c - c(1 - \rho(\mathbf{u})) \left(\sum_{k=1}^{q} \xi_k \nabla_x m_k + \xi_v \nabla_x v \right) + c\mathcal{A} \right] \\
\qquad - \nabla_y \cdot [(\mathbf{b}(y, \mathbf{m}) - \mathbf{d}(y))c] \\
\qquad + 2^{p+1} \phi(2y, c, v)c(t, x, 2y) - \phi(y, c, v)c(t, x, y) \\
\frac{\partial v}{\partial t} = -\gamma_v^{\mathrm{T}} \mathbf{r} v + \psi_v(t, \mathbf{u}) \\
\frac{\partial \mathbf{m}}{\partial t} = \nabla_x \cdot [\mathbf{D_m} \nabla_x \mathbf{m}] - \int_{\mathcal{P}} \left(\hat{\mathbf{b}}(y, \mathbf{m}) - \hat{\mathbf{d}}(y) \right) \varepsilon c(t, x, y) \, \mathrm{d}y \\
\qquad + \psi_{\mathbf{m}}(\mathbf{u}, \mathbf{r}) - \mathrm{diag}\,(\gamma_{\mathbf{m}})\,\mathbf{m},
\end{cases}
\tag{3}
$$

where the bold vector notations are used here to represent

- The molecular population of unbound (free) part of the considered components of uPA system via $\mathbf{m} := [m_b^{\mathrm{T}}, m_f^{\mathrm{T}}]^{\mathrm{T}}$;
- The total molecular population (both bound and unbound part) of the considered components of uPA system via $\mathbf{r} := \left[\int_{\mathcal{P}} y\varepsilon c(t, x, y) \, \mathrm{d}y, \ \mathbf{m}(t, x) \right]^{\mathrm{T}}$,

and ε stands for the ratio between cell surface density and cancer cell density. Furthermore, to simplify the context, the cell cancer proliferation law $\phi(y, c, v)$ is chosen here to be of a non-structured logistic form, namely

$$\phi(y, \mathbf{u}) = \mu_c(1 - \rho(\mathbf{u})) \tag{4}$$

where $\rho(\mathbf{u})$ quantifies the space occupied by the ECM and total cancer cell density

$$C(t, x) := \int_{\mathcal{P}} c(t, x, y) \, \mathrm{d}y, \tag{5}$$

and is defined by

$$\rho(\mathbf{u}(t, x)) := \mathfrak{v}_c C(t, x) + \mathfrak{v}_v v(t, x) \tag{6}$$

with $\mathfrak{v}_c$ and $\mathfrak{v}_v$ denoting the volume fraction for c and v at the same spatio-temporal point (t, x), respectively. Moreover, the ECM remodelling term $\psi_v(t, \mathbf{u})$ assumes here the volume filling form

$$\psi_v(t, \mathbf{u}) := \mu_v(1 - \rho(\mathbf{u}))^+. \tag{7}$$

Finally, for the uPA binding components given by $m_b := [m_{b,1}, \ldots, m_{b,p}]^T$, the cell surface binding and unbinding rates are represented here by $\mathbf{b}(y, \mathbf{m})$ and $\mathbf{d}(y)$, respectively. Therefore, since for the free components m_f we do not have any binding or unbinding, to unify the notation, we use here the extended binding and unbinding rates vectors $\hat{\mathbf{b}}(y, \mathbf{m})$ and $\hat{\mathbf{d}}(y)$ in $\mathbb{R}^q$ given by

$$\hat{\mathbf{b}}(y, \mathbf{m}) := [(\mathbf{b}(y, \mathbf{m}))^T, 0, \ldots, 0]^T \text{ and } \hat{\mathbf{d}}(y) := [(\mathbf{d}(y))^T, 0, \ldots, 0]^T.$$

The molecular source $\psi_{\mathbf{m}}$ is assumed to depend here only on $\mathbf{u}$ and the total molecular population $\mathbf{r}$ while the constant vector $\gamma_{\mathbf{m}} \in \mathbb{R}^q$ represents the natural degradation rate of $\mathbf{m}$.

2.1 The Dynamics of uPA System with and Without PAI-1

Assuming that a total amount M of uPAR receptors is uniformly distributed on the surface of each cancer cell, in the following we explore the form and dynamics of the spatio-temporal-structural system (3) when considering uPA binding and unbinding to uPAR both in the presence and in the absence of binding PAI-1 inhibitor molecules. These will result in different structural dimensionalities that will be addressed below as appropriate.

2.1.1 uPA System in the Absence of PAI-1

The first case that we consider here accounts only for the uPA binding and unbinding molecules while ignoring the presence of PAI-1. In this context, the total number of considered uPA system components is $q = 2$ and consists of

- A binding molecular species (*i.e.*, uPA) represented by $m_b(t, x) := m_{b,1}(t, x)$;
- A free molecular species (*i.e.*, plasmin) represented by $m_f(t, x) := m_{f,1}(t, x)$.

The amount of those uPA molecules among $m_{b,1}(t, x)$ that are exercising binding to the available uPAR receptors is denoted here with y and represents the binding structure of the cancer cell population distributed at the spatio-temporal node (x, t). Thus, under the assumption of a certain level of membrane binding saturation, after eventual normalisation, the collection of all the binding structures $\mathcal{P}$ is given here by the interval $[0, 1]$, so the dimension of $\mathcal{P}$ is in this case $p = 1$. Furthermore, after a brief calculation (Domschke et al. 2017), the uPA binding rate $\mathbf{b}(y, \mathbf{m})$ is given by

$$\mathbf{b}(y, \mathbf{m}) = (1 - y)m_{b,1}, \tag{8}$$

while the uPA unbinding rate $\mathbf{d}(y)$ has a form

$$\mathbf{d}(y) = d_{m_{b,1}}y. \tag{9}$$

Furthermore, assuming that the unbound uPA is produced by the cancer cells $C(t, x)$ at the rate $\alpha_{m_{b,1}}$ and that plasmin is produced only by those cells which are bound by uPA at a rate $\alpha_{m_{f,1}}$, the molecular source term $\psi_{\mathbf{m}}(C, \mathbf{r})$ is given here by

$$\psi_{\mathbf{m}}(C, \mathbf{r}) = \left[\begin{array}{c} \alpha_{m_{b,1}} C \\ \alpha_{m_{f,1}} \int\limits_{\mathcal{P}} y \varepsilon c(t, x, y)\, \mathrm{d}y \end{array} \right]. \tag{10}$$

2.1.2 uPA System in the Presence of PAI-1

Building on the first modelling case assumed in Sect. 2.1.1, we consider now a second situation in which, besides the binding of uPA, the inhibitor PAI-1 is brought into the picture; this being able to bind to cell surface-bound uPA molecules, inhibiting their action. In this new context, the total number of molecular species in the uPA system considered is $q = 3$, this consisting of

- Two binding molecular species (uPA and PAI-1) represented by $m_b(t, x) :=$ $[m_{b,1}(t, x), m_{b,2}(t, x)]^{\mathrm{T}}$, with $m_{b,1}(t, x)$ standing for the unbound uPA density and $m_{b,2}(t, x)$ denoting the unbound PAI-1 inhibitor density;
- A free molecular species (*i.e.*, plasmin) represented by $m_f(t, x) := m_{f,1}(t, x)$.

While proceeding as in Sect. 2.1.1 and denoting amount of those uPA molecules among $m_{b,1}(t, x)$ that are exercising binding to the available uPAR receptors is denoted here with y_1, we denote with y_2 the amount of PAI-1 ligands that bind bound uPA, causing the inhibition of these uPA–uPAR complexes. Thus, given the binging possibilities for PAI-1 onto receptor-bound uPA versus the binding possibilities of the free uPA on the uPAR receptors, it is always the case that $y_2 \leq y_1$, and so after an eventual normalisation due to reaching saturation levels of cell surface uPA binding, we obtain that that maximal set of binding structures $\mathcal{P}$ is two-dimensional in this case and is given by $\mathcal{P} := \{(y_1, y_2) \in \mathbb{R}^2 \mid y_1 \in [0, 1] \text{ and } y_2 \in [0, y_1]\}$. Thus, using a measure theoretical argument (Domschke et al. 2017) for the binding components for the uPA and PAI-1, the vector of binding rates $\mathbf{b}(y, \mathbf{m})$ is given by

$$\mathbf{b}(y, \mathbf{m}) = \left[\begin{array}{c} (1 - y_1)\beta_1 m_{b,1} \\ (y_1 - y_2)\beta_2 m_{b,2} \end{array} \right] \tag{11}$$

and, similarly, we obtain that the vector of unbinding rates $\mathbf{d}(y)$ is

$$\mathbf{d}(y) = \left[\begin{array}{c} (y_1 - y_2)d_{y_1} \\ y_2 d_{y_2} \end{array} \right]. \tag{12}$$

Assuming that the uPA density $m_{b,1}$ is produced in the presence of cells expressing uPAR (namely the total cell density C) at a rate $\alpha_{m_{b,1}}$, $m_{b,2}$ is produced in the presence of activated plasminogen (namely the plasmin density $m_{f,1}$) at a rate $\alpha_{m_{b,2}}$, and plasmin density $m_{f,1}$ is activated by cells expressing uPA density $m_{b,1}$ but not also inhibitor PAI-1 density $m_{b,2}$ at a rate $\alpha_{m_{f,1}}$, we obtain that the molecular source term $\psi_{\mathbf{m}}$ is given by

$$\psi_{\mathbf{m}}(C, \mathbf{r}) = \left[\begin{array}{c} \alpha_{m_{b,1}} C \\ \alpha_{m_{b,2}} m_{f,1} \\ \alpha_{m_{f,1}} \int\limits_{\mathcal{P}} (y_1 - y_2)\varepsilon c(t, x, y)\, \mathrm{d}y \end{array} \right]. \tag{13}$$

3 Computational Approach and Analysis of the Discretisation of the Spatio-Structural-Temporal Tumour Model

Throughout this section, we consider only the case of one dimension in both space and structure for system (3). Thus, assuming equal spatial and structural step size $\delta_x = \delta_y$ and an equal number $r \in \mathbb{N} \setminus \{0, 1, 2, 3\}$ of collocation points in both x and y dimensions, in the following we will proceed to discretise c, v, and $\mathbf{m}$ at any given time node $n\delta_t$, with $n \in \mathbb{N}$. At each discretised spatial location in x, let c_x^n denote the vector of the discretisation of the distribution of the cancer cell population over the structural dimension y, explicitly given by $c_x^n := [c_{x,y_1}^n, \ldots, c_{x,y_r}^n]^{\mathrm{T}}$. Likewise, at each discretised structural location in y, let c_y^n denote the vector of the discretisation of the distribution of the cancer cell population over the spatial dimension x, explicitly given by $c_y^n := [c_{x_1,y}^n, \ldots, c_{x_r,y}^n]^{\mathrm{T}}$. In a similar way, the spatial discretisation of the ECM concentration is denoted by $v^n := [v_{x_1}^n, \ldots, v_{x_r}^n]^{\mathrm{T}}$. Further, to simplify the notation for the components of $\mathbf{m}$, in this section we will drop the indices $_b$ and $_f$ and orderly relabel the involved molecular species simply upon their position in the vector $\mathbf{m}$, namely as $\mathbf{m} = [m_1, \ldots, m_q]^{\mathrm{T}}$. In this context, the discretisation of $\mathbf{m}$ is simply denoted by $\mathbf{m}^n := [(m_1^n)^{\mathrm{T}}, \ldots, (m_q^n)^{\mathrm{T}}]^{\mathrm{T}} \in \mathbb{R}^{qr}$, with $m_i^n := [m_{i,x_1}^n, \ldots, m_{i,x_r}^n]^{\mathrm{T}}$, $\forall i \in \{1, \ldots, q\}$.

Finally, for appropriately designed $r \times r$ diagonal matrices Γ (aimed to serve for approximating expectations of the various structurally distributed variables that are involved in system (3)), let us denote $C^n(\Gamma) := [C_{x_1}^n(\Gamma), \ldots, C_{x_r}^r(\Gamma)]^{\mathrm{T}} \in \mathbb{R}^r$, with each component defined by

$$C_{x_i}^n(\Gamma) := \tfrac{\delta_y}{2}[c_{x_i}^n]^{\mathrm{T}} \Gamma [1, 2, 2, \ldots, 2, 2, 1]^{\mathrm{T}}, \tag{14}$$

and note that for instance the total cell density is given by $C(I_r)$, where I_r is the $r \times r$ identity matrix.

3.1 Discretisation of the 1D-Spatial 1D-Structural uPA Model

The iterative time step for the cancer population equation in (3) is then given by

$$c^{n+1} = c^n + \delta_c^n \quad \text{with} \quad \delta_c^n = (A_x c_x^n + (A_y + A_\phi) c_y^n) \cdot \delta_t \tag{15}$$

where

$$A_x = \tfrac{1}{4\delta_x^2} J^2 + \tfrac{1}{2\delta_x} J \tilde{f} \tag{16}$$
$$\tilde{f} := \mathrm{diag}([f_1, \ldots, f_r]),$$

with J_r being the $r \times r$ central difference derivative matrix given by

$$J_r = \begin{pmatrix} -2 & 2 & 0 & \dots & 0 & 0 & 0 \\ -1 & 0 & 1 & \dots & 0 & 0 & 0 \\ 0 & -1 & 0 & \ddots & 0 & 0 & 0 \\ \vdots & \vdots & \ddots & \ddots & \ddots & \vdots & \vdots \\ 0 & 0 & 0 & \ddots & 0 & 1 & 0 \\ 0 & 0 & 0 & \dots & -1 & 0 & 1 \\ 0 & 0 & 0 & \dots & 0 & -2 & 2 \end{pmatrix}, \tag{17}$$

and the components of $\tilde{f}$ being given by

$$f_i := f_i(c_{x_i}^n, v_{x_i}^n, \mathbf{m}_{x_i}^n) = \left(1 - \rho(c_{x_i}^n, v_{x_i}^n)\right) \left(\sum_k \xi_k \text{row}_i(J_r^2) \mathbf{m}_{k,x_i}^n + \xi_v \text{row}_i(J_r^2) v_{x_i}^n \right), \tag{18}$$

where $\text{row}_i(J_r^2)$ indicates the ith row of the matrix given by J_r^2, for all $i \in \{1, \dots, r\}$. Furthermore, we have that

$$A_y = -\frac{1}{2\delta_y} J_r \tilde{g}$$
$$\tilde{g} := \text{diag}([(b_1 - d_1), \dots, (b_r - d_r)]), \tag{19}$$

where $b_i := b(\mathbf{m}^n, y_i)$ and $d_i := d(y_i)$, $\forall i \in \{1, \dots, r\}$ stands for the discretised binding and unbinding rates, and

$$A_\phi = A_{\phi_y} + A_{\phi_{2y}} \tag{20}$$

with

$$A_{\overline{\phi_y}} = -\tilde{\phi}_y \qquad\qquad A_{\overline{\phi_{2y}}} = 2^{P+1} \hat{I}^{\text{T}} \tilde{\phi}_{2y} \hat{I}$$
$$\tilde{\phi}_y = \text{diag}([\phi_1, \dots, \phi_r]) \quad \tilde{\phi}_{2y} = \sum_{i=1}^r \phi_{2i} E_{i,2i} \quad \hat{I} = \begin{pmatrix} I_r \\ \text{Ø}_r \end{pmatrix}, \tag{21}$$

where Ø_r is the $r \times r$ zero matrix, $E_{i,2i}$ is the standard elementary matrix; $\phi_i := \phi(y_i, c_{y_i}^n, v^n)$ and $\phi_{2i} := \phi(2y_i, c_{2y_i}^n, v^n)$, $\forall i \in \{1, \dots, r\}$.

Similarly iterative time step for the ECM equation in (3) is given by

$$v^{n+1} = v^n + \delta_v^n \quad \text{with} \quad \delta_v^n = (B_x v^n + \tilde{\psi}_v) \cdot \delta_t, \tag{22}$$

where

$$B_x = -\gamma_{v,c} \varepsilon \text{diag}(C^n(\tilde{y})) - \sum_{i=1}^q \gamma_{v,m_i} \text{diag}(m_i^n), \tag{23}$$

with $\tilde{y} := \text{diag}([y_1, \dots, y_r])$, the ECM degradation rates vector γ_v organised as $\gamma_v := [\gamma_{v,c}, \gamma_{v,m_1}, \dots, \gamma_{v,m_q}]^{\text{T}}$. Furthermore, $\tilde{\psi}_v$ denotes here the remodelling vector given by

$$\tilde{\psi}_v := [\psi_{v,1}, \dots, \psi_{v,r}]^{\text{T}}, \tag{24}$$

where we use the reduced notation $\psi_{v,i} := \psi_v(c_i^n, v_i^n)$, $\forall i \in \{1, \ldots, r\}$.

Finally, the iterative time step for uPA components equation in (3) is given by

$$\mathbf{m}^{n+1} = \mathbf{m}^n + \delta_\mathbf{m}^n \text{ with } \delta_\mathbf{m}^n = (D_x(\mathbf{m}^n) + D_\phi) \cdot \delta_t, \tag{25}$$

where we used the operator notation $D_x(\mathbf{m}^n) := [(D_{m_1} J_r^2 m_1^n)^\mathrm{T}, \ldots, (D_{m_q} J_r^2 m_q^n)^\mathrm{T}]^\mathrm{T}$, and

$$D_{\phi_i} := \psi_{m_i} - \varepsilon C^n(\tilde{g}) - \gamma_{m_i} m_i^n \tag{26}$$

where $\psi_{m_i} := [\psi_{m_i}(C_{x_1}^n(I_r), C_{x_1}^n(\tilde{y})), \ldots, \psi_{m_i}(C_{x_r}^n(I_r), C_{x_r}^n(\tilde{y}))]^\mathrm{T}$, $\forall i \in \{1, \ldots, q\}$, where we used the operator notation $D_\phi(\mathbf{m}^n) := [D_{\phi_1}^\mathrm{T}, \ldots, D_{\phi_q}^\mathrm{T}]^\mathrm{T}$.

Therefore, the first iteration of the resulting discrete *global operator* for an arbitrary discrete spatio-structural points (x, y), and time node $n = 0$, which appears when computing given by $(c^1, v^1, \mathbf{m}^1)^\mathrm{T}$, leads to the following *relations*:

$$
\begin{aligned}
\delta_c^0 &= \left(\tfrac{1}{4\delta_x^2} J_r^2 c_y^0 + \tfrac{1}{2\delta_x} J_r \tilde{f} c_y^0 - \tfrac{1}{2\delta_y} J_r \tilde{g} c_x^0 + \left(2^{P+1} \hat{I}^\mathrm{T} \tilde{\phi}_{2y} \hat{I} - \tilde{\phi}_y\right) c_y^0\right) \delta_t \\
\delta_v^0 &= \left(-\gamma_{v,c} \varepsilon \mathrm{diag}(C^n(\tilde{y})) v^0 - \sum_{k=1}^q \gamma_{v,m_k} \mathrm{diag}(m_k^n) v^0 + \tilde{\psi}_v\right) \delta_t \\
\delta_{m_k}^0 &= \left(D_{m_k} J_r^2 m_k^n + \psi_{m_k} - \varepsilon C^0(\tilde{g}) - \gamma_{m_k} m_k^n\right) \delta_t.
\end{aligned}
\tag{27}
$$

The stability of the primary term in these discrete time differences is dependent upon the operator J_r whose analysis will be the focus of the following subsection.

3.2 Stability Analysis Considerations on the Central Difference Operator J_r

In order to assess the stability of the difference operator J_r involved in (43), in the following we will prove a series of technical results that will ultimately completely characterise the eigenvalues of J_r.

Lemma 1 *Let $\mathcal{Q}$ be the following set of polynomials with real coefficients*

$$\mathcal{Q} := \left\{ P_k(x) = a_k x^k + \cdots + a_1 x + a_0 \left| \begin{array}{l} k \geq 4, \\ a_{k-1-2i} = 0, \ \forall i \in 0, \ldots, \left[\frac{k-1}{2}\right] \end{array} \right. \right\} \tag{28}$$

where by $[\cdot]$ we understand the usual integer part. Further, let $P_{N-2}, P_{N-1} \in \mathcal{Q}$ be polynomials of degree $N - 2$ and $N - 1$ respectively, then the iterative relation $P_N = P_{N-2} - x P_{N-1}$ gives rise to a polynomial of degree N with $P_N \in \mathcal{Q}$.

Proof If one writes the considered polynomials as

$$
\begin{aligned}
P_{N-2} &: a_{N-2} x^{N-2} + a_{N-4} x^{N-4} + \cdots + \max_{i \in \{0, \ldots, [\frac{k-1}{2}]\}} a_{N-i-3} x^{N-i-3} = 0 \\
P_{N-1} &: a_{N-1} x^{N-1} + a_{N-3} x^{N-3} + \cdots + \max_{i \in \{0, \ldots, [\frac{k-1}{2}]\}} a_{N-i-2} x^{N-i-2} = 0,
\end{aligned}
\tag{29}
$$

then the proof is trivial.   □

Theorem 1 *Considering the set of polynomials $\mathcal{Q}$ defined in (28), for any natural $N \geq 6$, let $P_N \in \mathcal{Q}$ be a polynomial of degree N such that the polynomials $P_{N-2}, P_{N-1} \in \mathcal{Q}$ that give P_N via the recurrence relation $P_N = P_{N-2} - x P_{N-1}$ satisfy the following properties:*

(1) *denote $\{u_1, u_2, \ldots, u_{N-2}\}$ and $\{v_1, v_2, \ldots, v_{N-1}\}$ the ordered set of roots of the polynomials P_{N-2} and P_{N-1}, respectively*
(2) *the roots of these two polynomials are only imaginary, namely:*

$$Re(u_i) = 0 \quad \forall i \in \{1, \ldots, N-2\}$$
$$Re(v_j) = 0 \quad \forall j \in \{1, \ldots, N-1\}$$

(3) *finally, the roots of these two polynomials satisfy the additional relations:*

$$v_{N-1}^2 \geq u_{N-2}^2$$
and
$$u_i^2 \geq v_i^2 \geq u_{i-2}^2 \geq v_{i-2}^2, \quad \forall i \in \left\{ i = 2j \mid j \in \left\{1, \ldots, \left[\tfrac{N-2}{2}\right]\right\}\right\},$$

where for any $i \in \{i = 2j \mid j \in \{1, \ldots, \left[\tfrac{N-2}{2}\right]\}\}$ we have that $u_{j-1} := \bar{u}_j$ and $v_{j-1} := \bar{v}_j$.

Then, if we let $\{w_1, w_2, \ldots, w_N\}$ denote the ordered set of roots for P_N, we have that

(i) *all the roots of P_N are imaginary, i.e.,*

$$Re(w_i) = 0, \quad \forall i \in \{1 \ldots N\},$$

(ii) *the roots of P_N and P_{N-1} satisfy the relations:*

$$w_{N-1}^2 \geq v_{N-2}^2$$
and
$$v_i^2 \geq w_i^2 \geq v_{i-2}^2 \geq w_{i-2}^2, \quad \forall i \in \left\{ i = 2j \mid j \in \left\{1, \ldots, \left[\tfrac{N-1}{2}\right]\right\}\right\},$$

where for any $i \in \{i = 2j \mid j \in \{1, \ldots, \left[\tfrac{N-1}{2}\right]\}\}$ we have that $w_{j-1} := \bar{w}_j$.

Proof First, we notice that there are 2 different cases:

(1) N is even or
(2) N is odd.

Take case (1) and let $N = 2n$, $n \in \mathbb{N}$. We can use the conjugate root theorem to write the polynomials as

$$P_{N-2}(x) = \left(x^2 - u_2^2\right)\left(x^2 - u_4^2\right)\ldots\left(x^2 - u_{N-2}^2\right)$$
$$P_{N-1}(x) = -x\left(x^2 - v_2^2\right)\left(x^2 - v_4^2\right)\ldots\left(x^2 - v_{N-2}^2\right),$$
(30)

where $u_{2i-1} = \overline{u_{2i}}$, $u_{2i}^2 = u_{2i-1} \cdot u_{2i}$ and $v_{2i-1} = \overline{v_{2i}}$, $v_{2i}^2 = -|\text{Im}(v_{2i})^2|$. We then have that P_N can be written as

$$P_N(x) = \left(x^2 - u_2^2\right)\left(x^2 - u_4^2\right)\ldots\left(x^2 - u_{N-2}^2\right)$$
$$+ x^2 \left(x^2 - v_2^2\right)\left(x^2 - v_4^2\right)\ldots\left(x^2 - v_{N-2}^2\right). \qquad (31)$$

Now, by Descartes' rule of signs and Lemma 1, we can say that none of the roots of P_N are positive and that at most N of these roots are negative.

Use the substitution $z = x^2$, the initial polynomial P_N induces

$$\bar{P}_N(z) = \left(z - u_2^2\right)\left(z - u_4^2\right)\ldots\left(z - u_{N-2}^2\right) + z\left(z - v_2^2\right)\left(z - v_4^2\right)\ldots\left(z - v_{N-2}^2\right). \qquad (32)$$

Evaluating $\bar{P}_N(z)$ at $\pm\infty$ and at a selection roots of $P_{N-1}(x)$ given by

$$S_a := \left\{v_{2j}^2 \mid j = 1, n-1\right\},$$

we have two different cases:

(1a) $n - 1$ is odd or
(1b) $n - 1$ is even.

In case (1a), we have that

$$\lim_{z \to \pm\infty} \bar{P}_N(z) = +\infty.$$

Further, as the elements of S_a are solutions of P_{N-1}, using their properties that $u_{2j}^2 \geq v_{2j}^2$, $j = 1, n$, we obtain

$$\bar{P}_N\left(v_{2j}^2\right) = (-1)^j \left|v_i^2 - u_2^2\right|\left|v_i^2 - u_4^2\right|\cdots\left|v_i^2 - u_{N-2}\right|, \qquad j = 1, n-1, \quad (33)$$

and so

$$\text{sign}\left(\bar{P}_N(v_{2j}^2)\right) = (-1)^j, \qquad j = 1, n-1$$

Therefore, denoting $S_a' := \{-\infty\} \cup S_a \cup \{+\infty\}$, we have

$$\text{sign}(\bar{P}_N(S_a')) = \{+, -, +, -, \cdots, -, +\}, \qquad (34)$$

which yields n intervals where the values of polynomial changes, and so by intermediate value theorem we must have n real non-positive roots for $\bar{P}_N(z)$.
Thus, reversing now the change of variable $z = x^2$, we obtain that the initial polynomial $P_N(x)$ has only imaginary roots with

$$\text{Re}(w_i) = 0 \quad with \quad w_i \geq v_i, \quad i = 1, N$$

For case (1b), we have that

$$\lim_{z \to \pm\infty} \bar{P}_N(z) = \pm\infty$$

Further, denoting by with S_b the following set of squares of the roots of $P_{N-2}(x)$, namely

$$S_b := \{u_{2j}^2 \mid j = 1, n - 1\},$$

$$\text{sign}(\bar{P}_N(u_{2j}^2)) = (-1)^{n-j}, \quad j = 1, n - 1$$

Therefore, denoting $S_b' := \{-\infty\} \cup S_b \cup \{+\infty\}$, we have

$$\text{sign}(\bar{P}_N(S_b')) = \{-, +, -, +, \cdots, -, +\}, \tag{35}$$

and by the intermediate value theorem, we again get $\text{Re}(w_i) = 0$ with $w_i \geq v_i$.

For case (2), we consider odd values of N and let $N = 2n + 1$, $n \in \mathbb{N}$ such that we again use the conjugate root theorem to write

$$P_{N-2}(x) = -x \left(x^2 - v_2^2\right) \left(x^2 - v_4^2\right) \ldots \left(x^2 - v_{N-2}^2\right)$$
$$P_{N-1}(x) = \left(x^2 - u_2^2\right) \left(x^2 - u_4^2\right) \ldots \left(x^2 - u_N^2\right)$$
$$P_N(x) = -x \left(x^2 - u_2^2\right) \left(x^2 - u_4^2\right) \ldots \left(x^2 - u_{n-2}^2\right) - x \left(x^2 - v_2^2\right) \left(x^2 - v_4^2\right) \ldots \left(x^2 - v_N^2\right). \tag{36}$$

Further, factoring out the common multiple $-x$ and using the substitution $z = x^2$ to augment the remainder of the polynomial, we can now test the polynomial with the set, S', in the same way as in case (1). □

Theorem 2 *Assuming that N is the number of discretisation points and $N \geq 6$, the characteristic polynomials $P_N(\lambda)$ of the central differences matrices J_N satisfy the following recurrence relation*

$$P_N(\lambda) = P_{N-2}(\lambda) - \lambda P_{N-1}(\lambda).$$

Proof Let's denote P_N is the characteristic polynomial of the $N \times N$ dimensional central differences matrix, J_N, we observe first that desired the recurrence relation $P_N = P_{N-2} - \lambda P_{N-1}$ is trivially satisfied by the characteristic polynomials of J_4, J_5, and J_6, which are given by

$$P_4 = \lambda^4 + \lambda^2$$
$$P_5 = -\lambda^5 - 2\lambda^3 \tag{37}$$
$$P_6 = \lambda^6 + 3\lambda^4 + \lambda^2.$$

To prove that this relation is satisfied in general for any natural number $N \geq 6$, we proceed as follows. First, $\forall l \in \mathbb{N} \setminus \{0, 1, 2, 3\}$, for the matrix $\hat{J}_l := J_l - \lambda I_l$, and let us

denote by A_l^o and A_l' the following determinants of the $(l-1) \times (l-1)$ submatrices of $\hat{J}_l$, namely

$$
A_{l-1}^o = \begin{vmatrix}
\hat{J}_{2,2} & \hat{J}_{2,3} & \hat{J}_{2,4} & \dots & \hat{J}_{2,l} \\
\hat{J}_{3,2} & \hat{J}_{3,3} & \hat{J}_{3,4} & \dots & \hat{J}_{3,l} \\
\hat{J}_{4,2} & \hat{J}_{4,3} & \hat{J}_{4,4} & \dots & \hat{J}_{4,l} \\
\vdots & \vdots & \vdots & \dots & \vdots \\
\hat{J}_{l,2} & \hat{J}_{l,3} & \hat{J}_{l,4} & \dots & \hat{J}_{l,l}
\end{vmatrix},
$$

$$
A_{l-1}' = \begin{vmatrix}
\hat{J}_{2,1} & \hat{J}_{2,3} & \hat{J}_{2,4} & \dots & \hat{J}_{2,l} \\
\hat{J}_{3,1} & \hat{J}_{3,3} & \hat{J}_{3,4} & \dots & \hat{J}_{3,l} \\
\hat{J}_{4,1} & \hat{J}_{4,3} & \hat{J}_{4,4} & \dots & \hat{J}_{4,l} \\
\vdots & \vdots & \vdots & \dots & \vdots \\
\hat{J}_{l,1} & \hat{J}_{l,3} & \hat{J}_{l,4} & \dots & \hat{J}_{l,l}
\end{vmatrix},
$$

(38)

and let's observe that these have the properties that

$$
\begin{aligned}
A_{l-1}^o &= -\lambda A_{l-2}^o - A_{l-2}' \\
A_{i-1}' &= -A_{l-2}^o
\end{aligned}
$$

(39)

Then, using (39) we have that

$$
|\hat{J}_{N-2}| = (-2-\lambda)A_{N-3}^o - 2A_{N-3}'
\tag{40a}
$$

$$
\begin{aligned}
|\hat{J}_{N-1}| &= (-2-\lambda)A_{N-2}^o - 2A_{N-2}' \\
&= (-2-\lambda)(-\lambda A_{N-3}^o - A_{N-3}') - 2(-A_{N-3}^o) \\
&= (-2-\lambda)(-\lambda)A_{N-3}^o + (2+\lambda)A_{N-3}' + 2A_{N-3}^o \\
&= ((-2-\lambda)(-\lambda) + 2)A_{N-3}^o + (2+\lambda)A_{N-3}'
\end{aligned}
\tag{40b}
$$

$$
\begin{aligned}
|\hat{J}_N| &= (-2-\lambda)A_{N-1}^o - 2A_{N-1}' \\
&= (-2-\lambda)(-\lambda A_{N-2}^o - A_{N-2}') - 2(-A_{N-2}^o) \\
&= (-2-\lambda)(-\lambda(-\lambda A_{N-3}^o - A_{N-3}') - (-A_{N-3}^o)) + 2A_{N-2}^o \\
&= (-2-\lambda)(-\lambda(-\lambda A_{N-3}^o - A_{N-3}') - (-A_{N-3}^o)) \\
&\quad + 2(-\lambda A_{N-3}^o - A_{N-3}') \\
&= (-2-\lambda)(-\lambda)^2 A_{N-3}^o + (-2-\lambda)(-\lambda)A_{N-3}' \\
&\quad + (-2-\lambda)A_{N-3}^o - 2\lambda A_{N-3}^o - 2A_{N-3}' \\
&= ((-2-\lambda)(-\lambda)^2 + (-2-\lambda) - 2\lambda)A_{N-3}^o + ((-2-\lambda)(-\lambda) - 2)A_{N-3}'
\end{aligned}
\tag{40c}
$$

From (40a)–(40c), we obtain immediately by direct calculation that

$$
|\hat{J}_N| = |\hat{J}_{N-2}| - \lambda|\hat{J}_{N-1}|
\tag{41}
$$

which can finally be equivalently expressed as

$$P_N(\lambda) = P_{N-2}(\lambda) - \lambda P_{N-1}(\lambda). \tag{42}$$

$\square$

Therefore, we finally obtain the following central result for our analysis.

Theorem 3 *The eigenvalues of the central differences matrix J_r are either 0 or imaginary.*

Proof Using Theorem 2, we have that the characteristic polynomial of J_r is given by $P_r(\lambda)$ and that $u_i^2 \geq v_i^2 \geq u_{i-2}^2 \geq v_{i-2}^2$ for all $i \in \{i = 2j \mid j \in \{1, \ldots, [\frac{r-2}{2}]\}\}$. Then, by invoking Theorem 1, we immediately obtain by induction that the roots, denoted w_i, of characteristic polynomial of J_r are imaginary with $\text{Re}(w_k) = 0$, $\forall k \in \{1, \ldots, r\}$.

$\square$

3.3 Stability Analysis of the Global Numerical Scheme

Returning now to the stability analysis of the global numerical scheme associated with 1D-spatio-1D-structural case of (3), we will focus now only those operators occurring in (43) that have eigenvalues $\text{Re}(\lambda) > 0$. Therefore, as J_r was proved to be stable, of interest for the stability analysis remains the behaviour of the following remainders of the operators from (43) without those terms involving J_r that we indicate with $^-$, namely:

$$\bar{\delta}_c^0 = \left(2^{P+1}\hat{I}^T\tilde{\phi}_{2y}\hat{I} - \tilde{\phi}_y\right)c_y^0\delta_t$$
$$\bar{\delta}_v^0 = \left(-\gamma_{v,c}\varepsilon\text{diag}(C^n(\tilde{y}))v^0 - \sum_{k=1}^{q}\gamma_{v,m_k}\text{diag}(m_k^n)v^0 + \tilde{\psi}_v\right)\delta_t \tag{43}$$
$$\bar{\delta}_{m_k}^0 = \left(\psi_{m_k} - \varepsilon C^0(\tilde{g}) - \gamma_{m_k}m_k^n\right)\delta_t.$$

We begin by assessing the stability of the structural dimension by considering the mitotic operator for the 2nd and 3rd such iterations on c, wherein we have:

$$\bar{\delta}_c^1 = \left(A_{\overline{\phi_y}} + A_{\overline{\phi_{2y}}}\right)c_y^0\delta_t + \left(A_{\overline{\phi_y}} + A_{\overline{\phi_{2y}}}\right)^2 c_y^0\delta_t^2, \tag{44}$$

$$\bar{\delta}_c^2 = \left(A_{\overline{\phi_y}} + A_{\overline{\phi_{2y}}}\right)c_y^0\delta_t + \left(A_{\overline{\phi_y}} + A_{\overline{\phi_{2y}}}\right)^2 c_y^0\delta_t^2$$
$$+ \left(A_{\overline{\phi_y}} + A_{\overline{\phi_{2y}}}\right)^3 c_y^0\delta_t^3, \tag{45}$$

such that the nth iteration is given by

$$\bar{\delta}_c^n = \sum_{i=1}^{n+1}\left(A_{\overline{\phi_y}} + A_{\overline{\phi_{2y}}}\right)^i \delta_t^i c_y^0. \tag{46}$$

The basic criterion for stability is that a small perturbation in the solution will decrease or remain constant in value through time, $t \to \infty$. Now, since in the above sum, the order of the terms (with respect to δ_t) increases with i, we can form a preliminary estimate of the perturbation's growth using only the first $i = 1$ terms, namely

$$c^1_{x_i,y_j} = c^0_{x_i,y_j} + \left(-\phi_{y_j}c^0_{x_i,y_j} + 2^{P+1}\phi_{2y_j}c^0_{x_i,2y_j}\right) \cdot \delta_t \tag{47}$$

and so we get the following condition for stability

$$\phi_{y_j}c^n_{x_i,y_j} \geq 2^{P+1}\phi_{2y_j}c^n_{x_i,2y_j}. \tag{48}$$

Given that $0 \leq \phi \leq 1$, we have that for stability

$$\lim_{\delta_{y_j} \to 0} \lim_{y_j \to 0} c^n_{x_i,y_j} = \infty, \quad \forall n \in [0, N),$$
$$\lim_{\delta_{y_j} \to 0} \lim_{y_j \to \infty} c^n_{x_i,y_j} = 0, \quad \forall n \in [0, N). \tag{49}$$

Further, concerning the structural dynamics, denoting now by $\bar{\bar{\delta}}^n_{c;x_i,y_j}$ the change in the cancer cell distribution c due to the y-flux of the system at a given spatio-structural position (x_i, y_j) during a time interval $[n\delta_t, (n+1)\delta_t]$, we have that

$$\bar{\bar{\delta}}^0_{c;x_i,y_j} := A_y c^0_y \cdot \delta_t = \left(\tfrac{1}{2\delta_y}(b_{y_{j-1}} - d_{y_{j-1}})c^0_{x_i,y_{j-1}} - \tfrac{1}{2\delta_y}(b_{y_{j+1}} - d_{y_{j+1}})c^0_{x_i,y_{j+1}}\right) \cdot \delta_t. \tag{50}$$

Therefore, if we have that b, d are proportional to y, then we can extract the modified binding and unbinding rates $\check{b}$ and $\check{d}$ as

$$b^n_{y_j}(y_j, \mathbf{m}^n) = \check{b}(\mathbf{m}^n) \cdot y_j \text{ and } d_{y_j}(y) = \check{d} \cdot y_j, \tag{51}$$

and so we can then write

$$\bar{\bar{\delta}}^0_{c;x_i,y_j} = \left(y_{j-1}c^0_{x_i,y_{j-1}} - y_{j+1}c^0_{x_i,y_{j+1}}\right) \cdot \tfrac{1}{2\delta_y}(\check{b}^0 - \check{d}^0) \cdot \delta_t, \tag{52}$$

whose stability is ensured by having either

$$\check{b} \leq \check{d}, \tag{53a}$$

or

$$c^0_{x_i,y_{j-1}} \leq \frac{y_{y_{j+1}}}{y_{y_{j-1}}}c^0_{x_i,y_{j+1}}, \quad \forall x_i, y_j. \tag{53b}$$

Thinking biologically about the ramifications of the former constraint, (53a), this would mean that the unbinding of the molecular species involved was more frequent than the binding of these species which would imply a relationship of affinity that approaches 0. Although these exist biologically, the considered system is one in which the binding of molecular species plays a major role in the metabolic processes of the

cell and one can thusly disregard (53a) from consideration as trivial. Therefore, we consider here only (53b) as viable.

From (48), (49), and (53b), however, we have a contradiction and therefore, the system must be unstable with neither an absolute nor a convective instability. The instability present is absolute in its source but convective in its requirement and behaviour.

For the stability of the equation in v of the discretised 1D-spatio-1D-structural system (3), from (43) we observe first that $0 \leq c_{x_i, y_j}^n \leq 1$ and $0 \leq m_{k; x_i, y_j}^n$, $\forall k \in \{1, \ldots, q\}$. It is then trivial to show the following eigenvalues relations

$$
\begin{aligned}
\lambda_{\text{diag}(c_{x_i, y_j}^n)} &= c_{x_i, y_j}^n \geq 0, \\
\lambda_{\text{diag}(m_{k; x_i}^n)} &= m_{k; x_i}^n \geq 0, \quad \forall k \in \{1, \ldots, q\}, \\
\lambda_{B_x} &\leq 0
\end{aligned}
\tag{54}
$$

where $\lambda_{\text{diag}(c_{x_i, y_j}^n)}$ denote the eigenvalues of $\text{diag}(c_{x_i, y_j}^n)$, $\lambda_{\text{diag}(m_{k; x_i}^n)}$ are the eigenvalues of $\text{diag}(m_{k; x_i}^n)$, and λ_{B_x} represent the eigenvalues of B_x. Therefore, using a similar notation, since for the eigenvalues of B_ϕ, we have that $\lambda_{B_\phi} \geq 0$, given smooth solutions for c_x^n and m_x^n, we finally obtain that the solutions for v_x^n will remain smooth and stable.

Finally, using the similar eigenvalue notation, for the stability in the equations for **m**, we obtain that the eigenvalues for $C^n(\tilde{g})$, δ_m and $\tilde{\psi}_m$ have the properties

$$
\begin{aligned}
\lambda_{C^n(\tilde{g})} &\geq 0, \\
\lambda_{\delta_{\mathbf{m}}} &= \gamma_{\mathbf{m}}, \\
\lambda_{\tilde{\psi}_{\mathbf{m}}} &\geq 0.
\end{aligned}
\tag{55}
$$

Moreover, we can also observe that eigenvalues of D_ϕ have the property that

$$
\lambda_{D_\phi} \leq 0 \quad \text{iff} \quad \lambda_{\tilde{\psi}_{\mathbf{m}}} \leq \gamma_{\mathbf{m}} + \varepsilon \lambda_{C^n(\tilde{g})}.
\tag{56}
$$

where for convenience we used the vector convention in writing the above inequality, which simply means that the inequality is respected per each component. Thus, we have that either (1) $\tilde{\psi}_{\mathbf{m}}$ is proportional to $\varepsilon C^n(\tilde{g})$ or (2) $\tilde{\psi}_{\mathbf{m}}$ is proportional to $C^n(I_r)$. For case (1), if we let $k_{\psi, 1}$ be the proportionality constant within the relation $\psi_{\mathbf{m}}$, then we can write that there must exist some values for $C_x^n(\tilde{g})$ at which

$$
\begin{aligned}
k_{\psi, 1} \varepsilon \lambda_{C^n(\tilde{g})} &\leq \gamma_{\mathbf{m}} + \varepsilon \lambda_{C^n(\tilde{g})} \\
(k_{\psi, 1} - 1) \varepsilon \lambda_{C^n(\tilde{g})} &\leq \gamma_{\mathbf{m}} \\
(k_{\psi, 1} - 1) \varepsilon C^n(\tilde{g}) &\leq \gamma_{\mathbf{m}},
\end{aligned}
\tag{57}
$$

where we used the same vector convention as in (56). Thus, using integration by parts, we can write

$$
(k_{\psi, 1} - 1) \varepsilon \left(\tilde{g} C^n(I) - (\check{b} - \check{d}) y_r C^n(I_r) \right) \leq \gamma_{\mathbf{m}}.
\tag{58}
$$

For case (2), if we let $k_{\psi,2}$ be the proportionality constant within the relation $\psi_{\mathbf{m}}$ then we can write that there must exist some values for $C^n(I_r)$ at which

$$
\begin{aligned}
k_{\psi,2} \lambda_{C^n(I_r)} &\leq \gamma_{\mathbf{m}} + \varepsilon \lambda_{C^n(\tilde{g})} \\
k_{\psi,2} C^n(I) &\leq \gamma_{\mathbf{m}} + \varepsilon \left(\tilde{g} C^n(I) - (\check{b} - \check{d}) y_r C^n(I_r) \right) \\
k_{\psi,2} C^n(I_r) &\leq \gamma_{\mathbf{m}} + \varepsilon \left(\tilde{g} - (\check{b} - \check{d}) y_r \right) C^n(I_r)
\end{aligned}
\tag{59}
$$

where $\tilde{g} \geq (\check{b} - \check{d}) y_r$. Therefore, given sufficiently large values for $C^n(I_r)$, given by

$$
C^n(I_r) \leq \frac{\gamma_{\mathbf{m}}}{k_{\psi,2} - \varepsilon \left(\tilde{g} - (\check{b} - \check{d}) y_r \right)},
\tag{60}
$$

the solutions for m_i^n will be unstable with

$$
\lim_{n \to \infty} m_i^n = \infty \quad \forall i \text{ where } \psi_{m_i} = \psi_{m_i}(c_x^n, \cdot).
\tag{61}
$$

For sufficiently low values of $C^n(I_r)$, given by the contrary argument to (60), the solutions for m_i^n will be stable with $m_i^n = 0$.

4 Numerical Results and Simulations in 1D-Spatial Case

The parameters considered throughout this work are chosen to be consistent with those set out in Domschke et al. (2017), and other previous models Gerisch and Chaplain (2008), and are detailed in Appendix A.

Numerical results generated by running the test case, and finite difference scheme for the system, through MATLAB are given below (Figs. 1, 2, 3, 4, 5, 6, 7, 8, 9). Several different cases are simulated in order to numerically verify the validity of proposed changes to the system and in order to perform analyses of the system using numerically generated graphic results:

For the 1D-spatial, 1D-structural case the associated model (3) was explored numerically in the presence of initial conditions for $c(t, x, y)$ for $t = 0$, given by
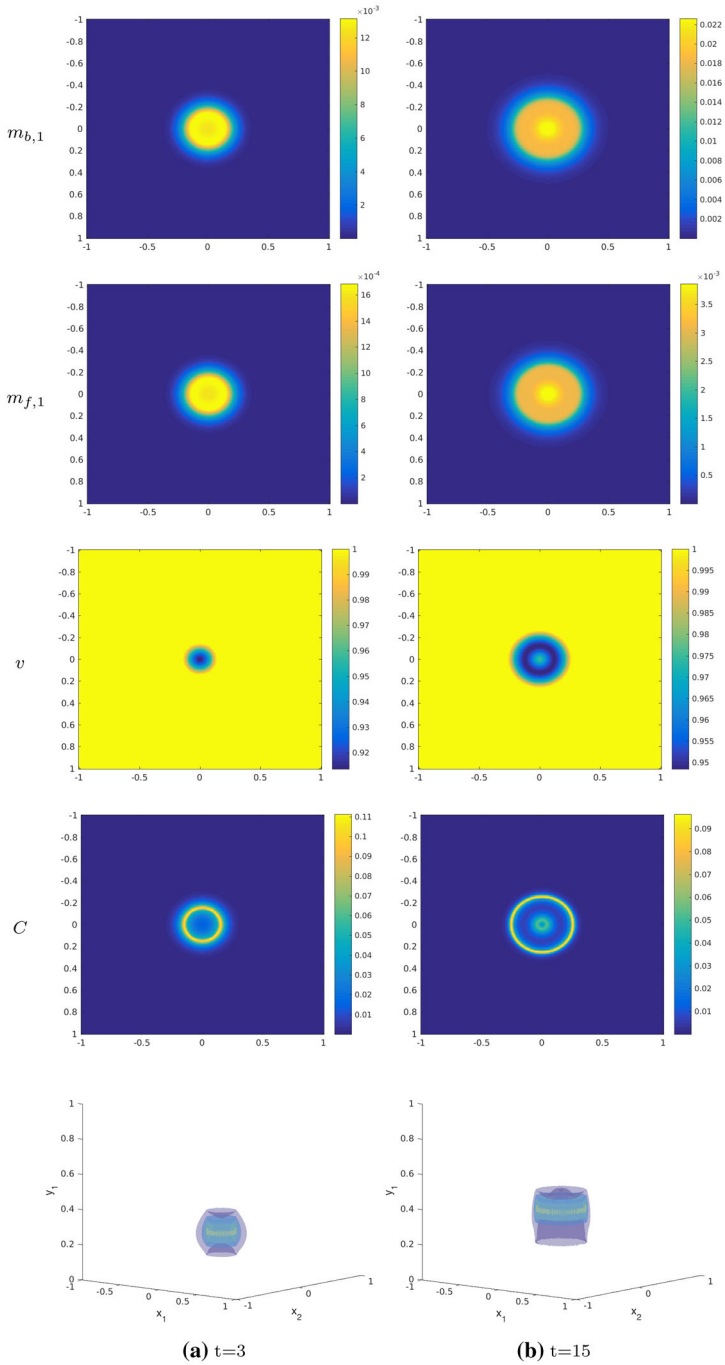
$$
c_0(x, y) := c(0, x, y) = \exp\left[-100 \left(x^2 + 4(y - \tfrac{1}{4})^2 \right) \right],
\tag{62}
$$

and the *homogeneous* ECM conditions

$$
v_0(x) := v(0, x) = 1 - \int_{\mathcal{P}} c(0, x, y) \, dy.
\tag{63}
$$
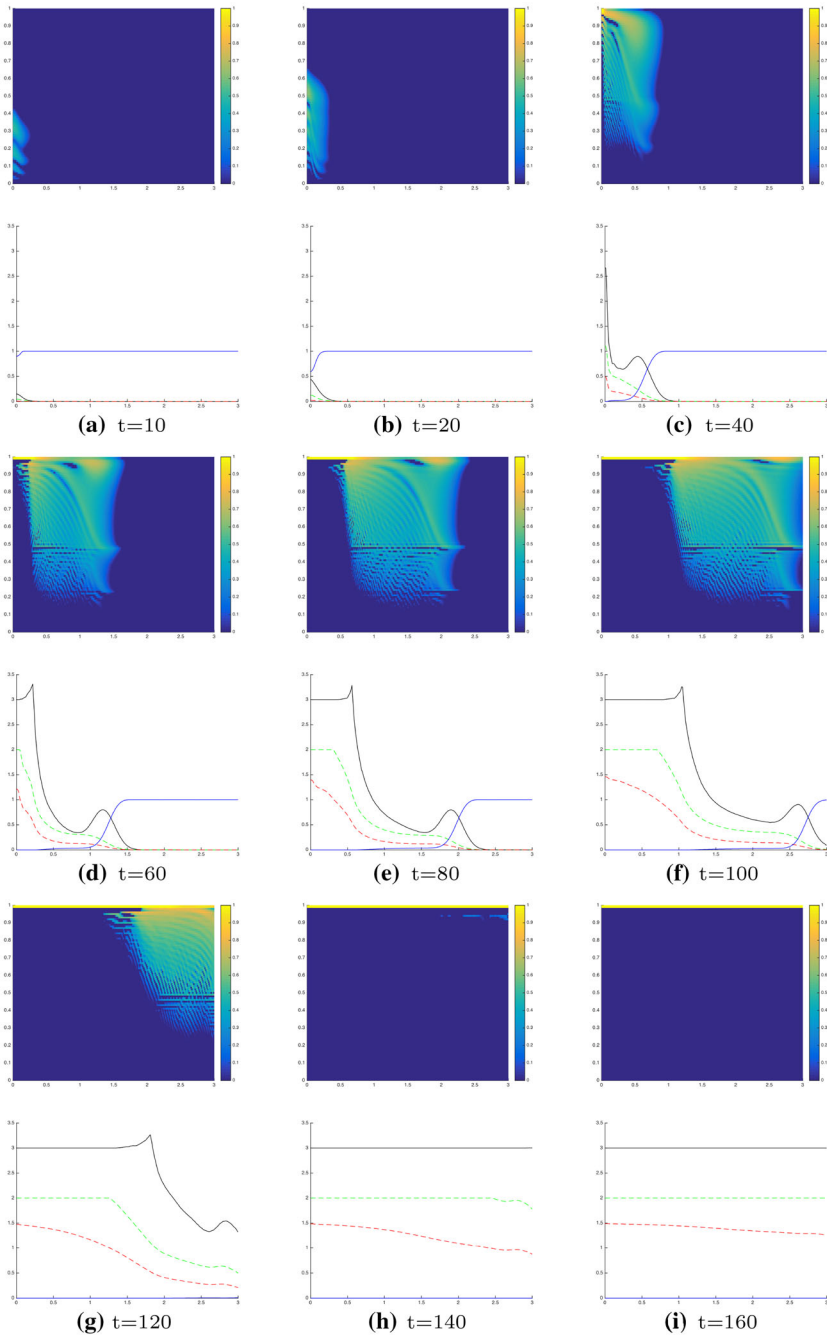
Fig. 1 Numerical 1D-spatial 1D-structural results generated from simulation of the system (3), with c plotted in the x- and y-dimension (top), with values for C (black), v (blue), $m_{b,1}$ (green dashed), and $m_{f,1}$ (red dashed) plotted spatially (bottom) (Color figure online)
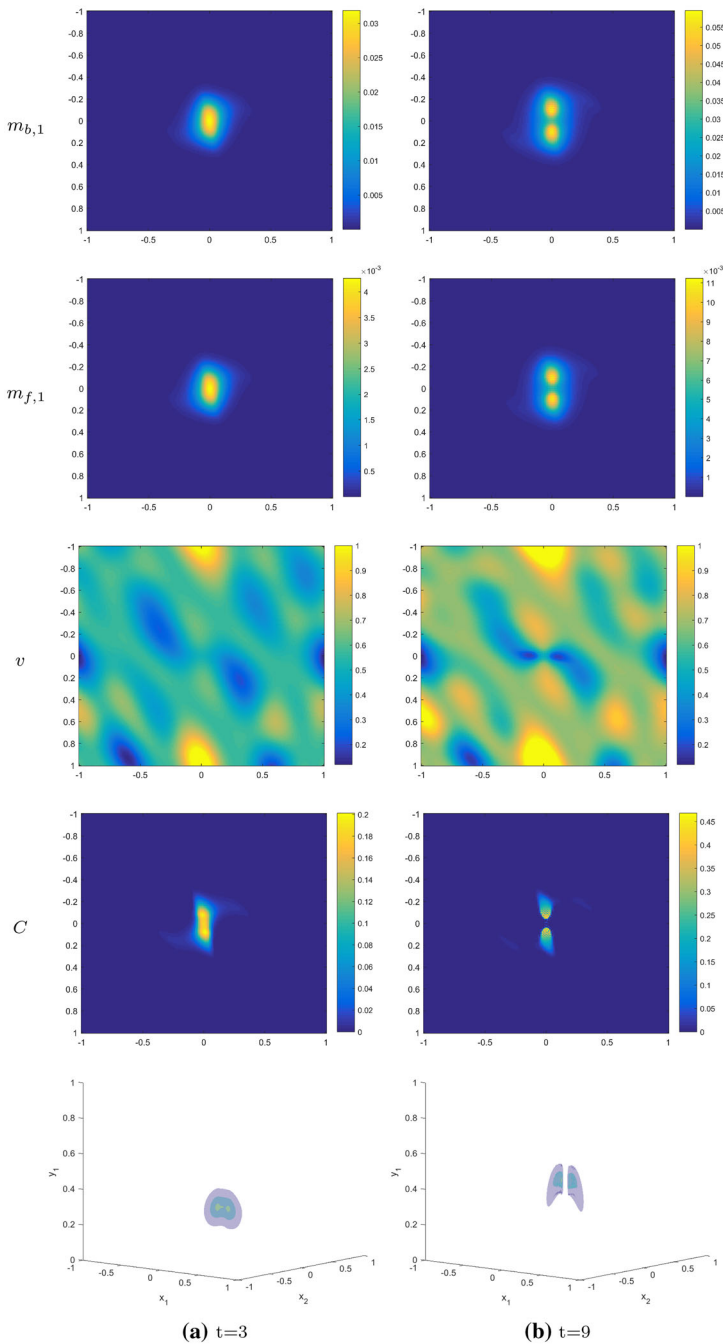
Fig. 2 Numerical 2D-spatial 1D-structural results for (3) for homogeneous ECM, plotted at times $t \in \{3, 15\}$: $m_{b,1}$ (row 1), $m_{f,1}$ (row 2) v (row 3), C (row 4), and c (row 5) as an isosurface on the 2D x-plane (Color figure online)
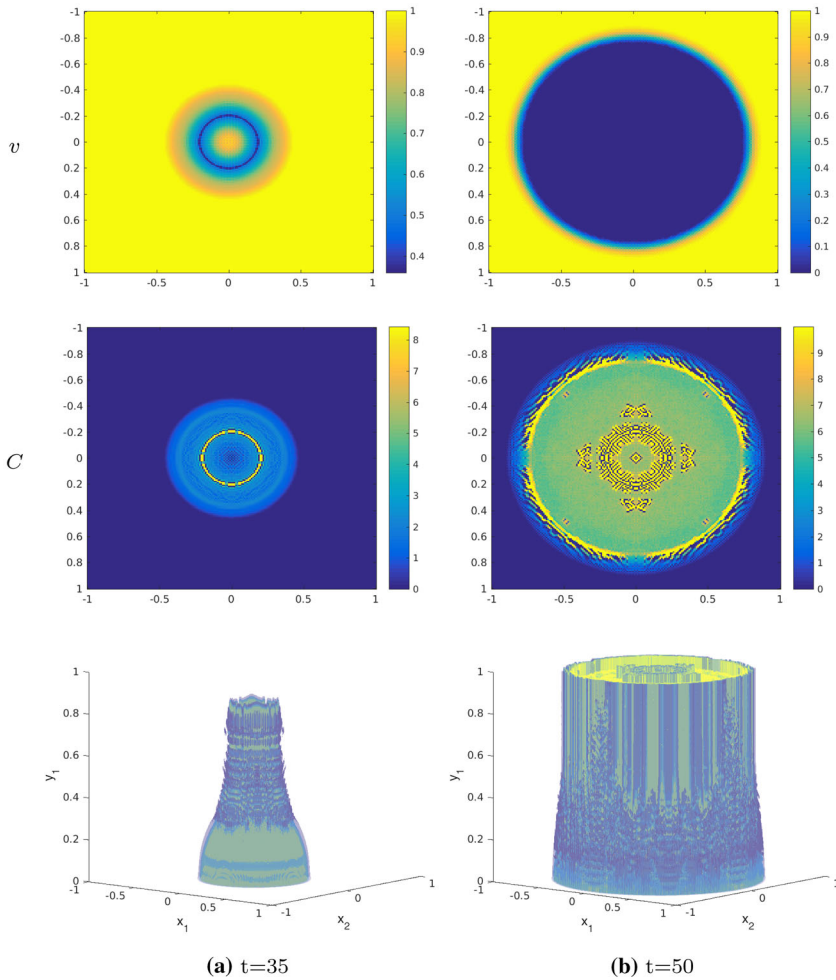
Fig. 3 Numerical 2D-spatial 1D-structural results for (3) for homogeneous ECM, plotted at times $t \in \{35, 50\}$: v (row 1), C (row 2), and c (row 3) as an isosurface on the 2D x-plane (Color figure online)

4.1 uPA in the Absence of PAI-1: 1D-Spatial 1D-Structural Results

One characteristic of the numerical solution, which has not previously been observed, is that of the partial travelling wave translation in the structural dimension (Fig. 1). That is to say that the proliferative terms lead to the travelling wave being depleted and replaced, to a greater extent at a lower value for y. These features shall be henceforth referred to as structural "y-waves" and is an essential feature in understanding the dynamics of such systems, given their recurrence in all domains. There is not sufficient evidence in the biological literature to verify that this is the case or to contradict this result.

The hyper-affinity binding also results in the behaviour of "replicative y-trapping" (referring to the behaviour of c collection at the upper y boundary as y-trapping and the

Fig. 4 Numerical 2D-spatial 1D-structural results for (3) for heterogeneous ECM, plotted at times $t \in \{3, 9\}$: $m_{b,1}$ (row 1), $m_{f,1}$ (row 2) v (row 3), C (row 4), and c (row 5) as an isosurface on the 2D x-plane (Color figure online)
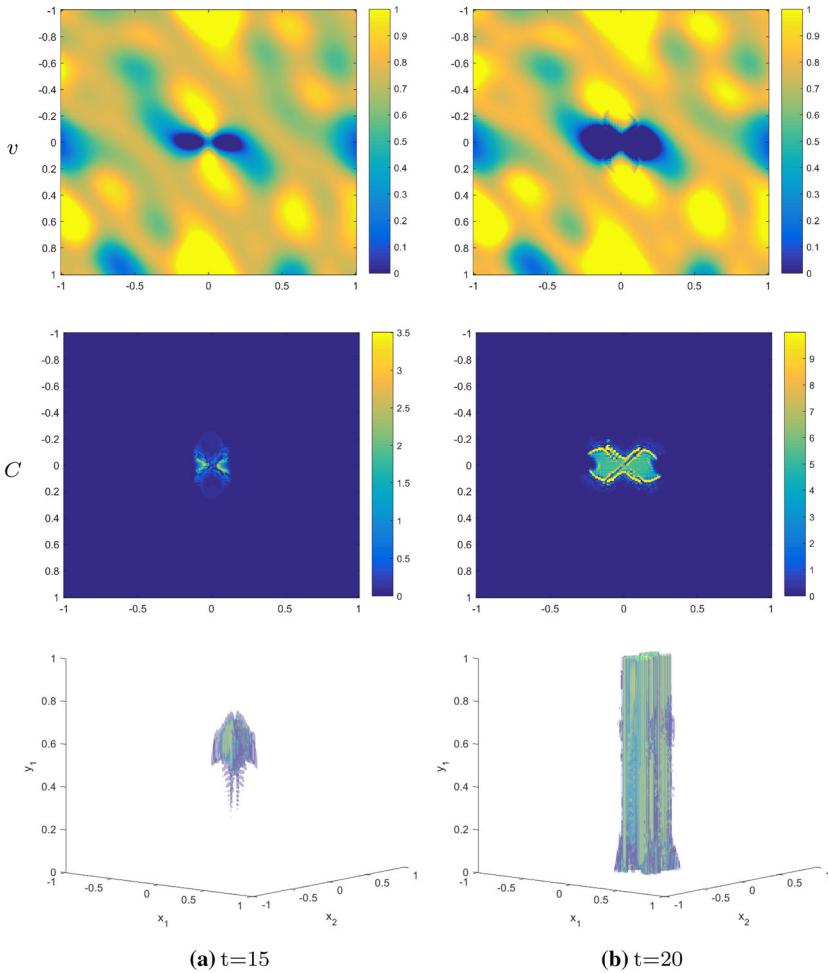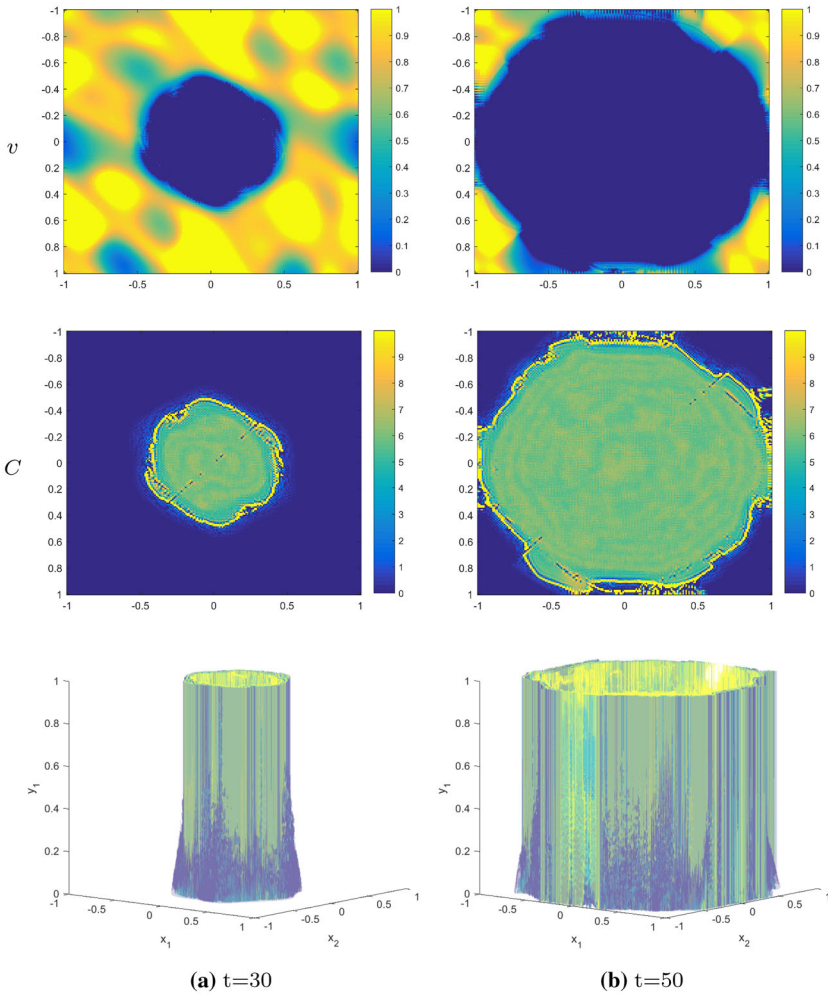
Fig. 5 Numerical 2D-spatial 1D-structural results for (3) for heterogeneous ECM, plotted at times $t \in \{15, 20\}$: v (row 1), C (row 2), and c (row 3) as an isosurface on the 2D x-plane (Color figure online)

proliferative duplication at $\frac{1}{2}y$ as replicative of this y-trapping) behaviour producing a discontinuity that fails to allow the system to continue the migration of c through $\mathcal{P}$ and raises significant questions of the biological efficacy of this system when coupled to assumptions of equal mitosis. Again, this results from the binding and production of these species occurring at far higher rates than the unbinding or degradation of these species.

The y-waves actually caused a resultant x-resolved profile, $C(t, x)$, which was itself not smooth (Fig. 1); this is a ramification of the proliferative contribution to the replication of steep gradient profiles. One must observe that, within the discrete space, the proliferative term necessarily means that any gradient is replicated with a proliferative constant, μ_c.
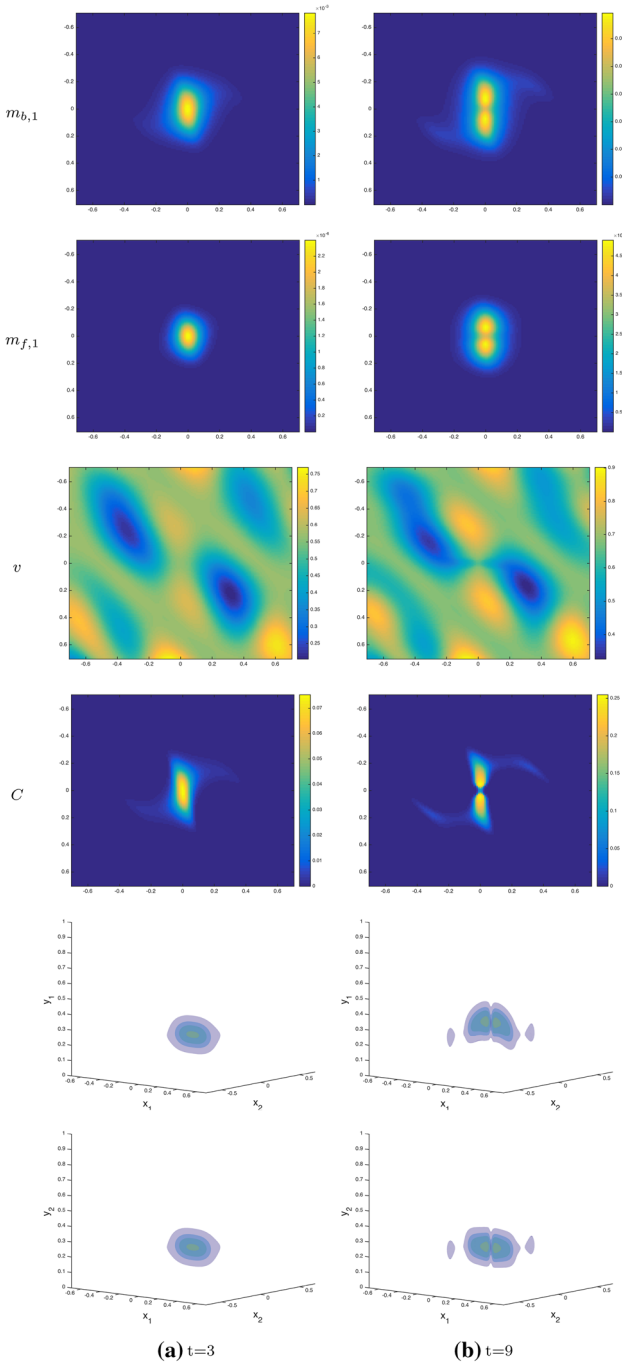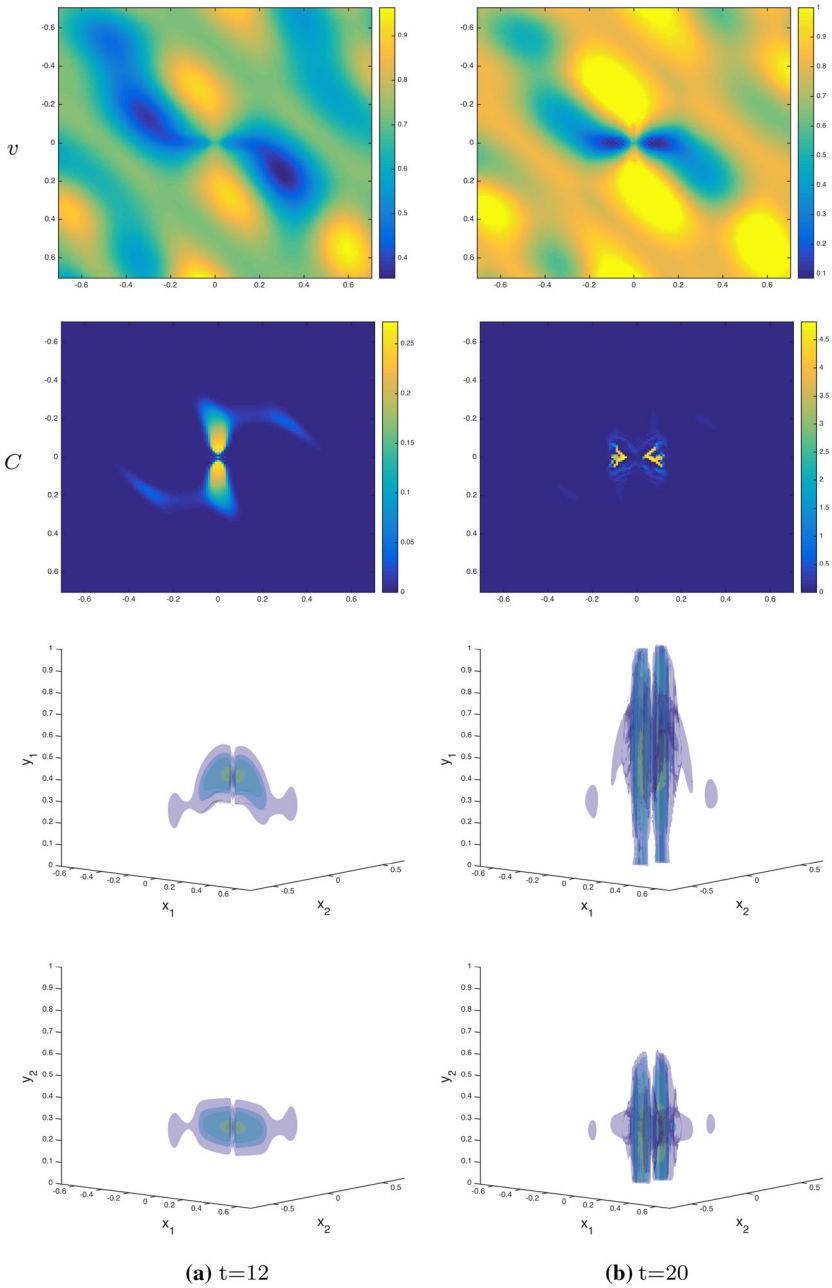
Fig. 6 Numerical 2D-spatial 1D-structural results for (3) for heterogeneous ECM, plotted at times $t \in \{30, 50\}$: v (row 1), C (row 2), and c (row 3) as an isosurface on the 2D x-plane (Color figure online)

Further, one observes an sharp spiking behaviour that occurs only at the boundary, which can be directly observed for $t = 50$ (Fig. 1c). The source of this spiking is not clear, since it occurs to a lesser extent for other values of (t, x), but could be due to the gradient-guided dissipation occurring only one side of the spike. In other words, the accuracy of the estimate of the double derivative is lessened by the fact that the peak occurs on the boundary and one can obtain information about the local features on only one side of the peak. It is also possible that this results from the contribution of the chemotaxis to the molecular species, on the bulk of the population, and the haptotaxis, on the exterior of the population.

There exists, however, some biological evidence to corroborate this behaviour as a natural process occurring due to the difference between forces between cell-cell

Fig. 7 Numerical 2D-spatial 2D-structural results for (3) for heterogeneous ECM, plotted at times $t \in \{3, 9\}$: $m_{b,1}$ (row 1), $m_{f,1}$ (row 2), v (row 3), C (row 4), $\int_{[0,1]} c \, dy_2$ (row 5) and $\int_{[0,1]} c \, dy_1$ (row 6) as isosurfaces on the 2D x-plane (Color figure online)

Fig. 8 Numerical 2D-spatial 2D-structural results for (3) for heterogeneous ECM, plotted at times $t \in \{12, 20\}$: v (row 1), C (row 2), $\int_{[0,1]} c\, dy_2$ (row 3) and $\int_{[0,1]} c\, dy_1$ (row 4) as isosurfaces on the 2D x-plane (Color figure online)

(a) t=25   **(b)** t=35
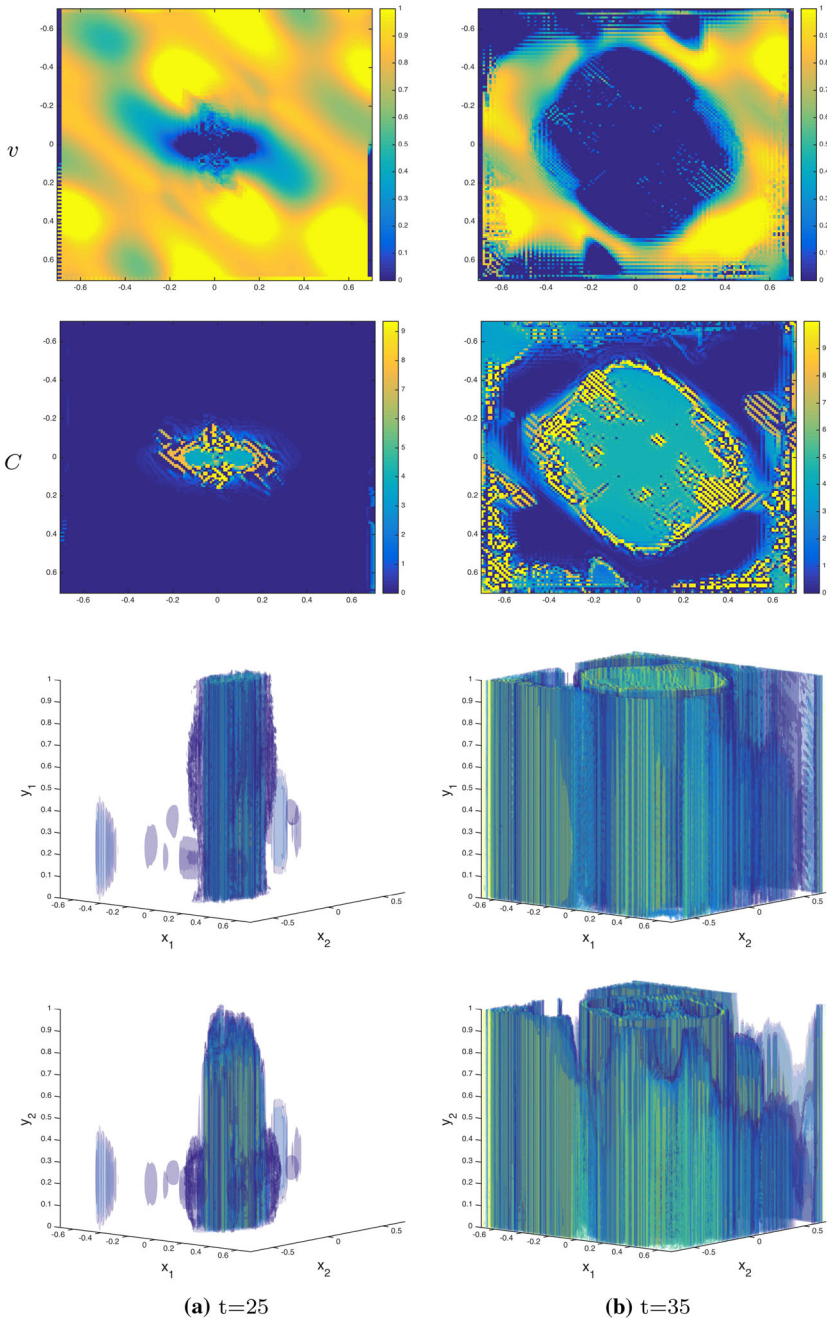
Fig. 9 Numerical 2D-spatial 2D-structural results for (3) for heterogeneous ECM, plotted at times $t \in \{25, 35\}$: v (row 1), C (row 2), $\int_{[0,1]} c \, dy_2$ (row 3) and $\int_{[0,1]} c \, dy_1$ (row 4) as isosurfaces on the 2D x-plane (Color figure online)

junctions and cell-ECM based motility. For instance, Yamaguchi et al. (2015) report the phenomenon of differential behaviours between 'leader' and 'follower' cells during collective cell migration, often resulting in a clustered cell subpopulation leading the migration of the tumour's boundary. Likewise, *in vivo* experimentation (necessarily invoking the heterogeneity of the underlying migratory substrate) has demonstrated breakaway clusters of cells which develop anterior to the invasive front (Chapman et al. 2014).

5 Numerical Results in 2D-Spatial Cases

Proceeding in a similar manner to the 1D-spatial case, also in the 2D-spatial cases, with the appropriate 1D- or 2D-structural domain $\mathcal{P}$, we assume equal spatial and structural step size $\delta_{x_i} := \delta_{y_j} := \delta_x$, $i, j \in \{1, 2\}$ and an equal number $r \in \mathbb{N}^*$ of collocation points in both spatial and structural dimensions, and in the following we will proceed to discretise c, v, and **m** at any given time node $n\delta_t$, with $n \in \mathbb{N}$.

For the 2D-spatial 1D-structural model, numerical results have been obtained for the initial condition for $c(t, x, y)$ which are the extension of (62), and in this case are given by

$$c_0(x, y) := c(0, x, y) = \exp\left[-100\left(\|x\|_2^2 + 4(y - \tfrac{1}{4})^2\right)\right], \tag{64}$$

Furthermore, for the ECM, we use both the *homogeneous* initial conditions given in (63) and a new set of *heterogeneous* initial conditions given as in Andasari et al. (2011), namely:

$$(x_1, x_2) := \frac{1}{3}\left(x + \frac{3}{2}\right) \in [0, 1]^2 \text{ for } x \in \mathcal{D}, \ \ \zeta := 6\pi,$$

$$h(x_1, x_2) := \frac{1}{2} + \frac{1}{2}\sin\left(\frac{\zeta x_1}{x_2 + 1}\right)\sin(\zeta x_1 x_2)\sin\left(\frac{\zeta(1 - x_1)}{x_2 + 1}\right)\sin(\zeta(x_1 - 1)(x_2 - 1)),$$

$$v_0(x) := v(0, x) = \min\left\{h(x_1, x_2), \frac{1 - \mathfrak{v}_c C(0, x)}{\mathfrak{v}_v}\right\}. \tag{65}$$

Finally, for the 2D-spatial 2D-structural model, numerical results have been obtained for the appropriate extension of the initial conditions for $c(t, x, y)$ considered in (62) and (64) which in this case recast as follows:

$$c_0(x, y) := c(0, x, y) = \exp\left[-100\left(\|x\|^2 + 4\|(y - [\tfrac{1}{4}, \tfrac{1}{4}]^\mathrm{T})\|^2\right)\right], \tag{66}$$

as well as the homogeneous and heterogeneous ECM initial conditions given in (63) and (65).

5.1 uPA in the Absence of PAI-1: 2D-Spatial 1D-Structural Results

Results from the simulations were consistent with the 1D-spatial 1D-structural case but varied widely due to the effect of the ECM on the cancer species.

Results for the 2D-spatial 1D-structural system for lower binding values are given (Figs. 2, 3). For *c*, the spatial distribution of the tumour in 2-spatial dimensions and

isosurface figure in a 2D-spatial 1D-structural domain (in the absence of PAI-1) are displayed to attempt to give the fullest impression of the progress of the cancer through the spatial and structural domains in time. One can see, again, the y-wave behaviour in the 2D-spatial system with mushroom-like forms replicating themselves at progressively lower values for y. A typical symmetric cancer cluster grows into the spatial domain, giving higher values for concentration at the upper boundary of $\mathcal{P}$ towards the epicentre of the cancer cluster.

In biological terms, this indicates that the more established, inner, portion of the tumour will likely have a higher bound population of molecules that the boundary, outer, portion. This result is counter-intuitive since, given that these bound species are more effective at degrading the extracellular matrix, a theoretical postulation might lead one to believe that these species would exist to a greater extent on the boundary. This is either a flaw within the application of the model or may provide an interesting observation about the efficiency of natural biological cancers.

Biological evidence does exist, on the other hand, to support the claim that both uPAR, and consequently surface bound uPA, are more highly concentrated towards the interior of invasive cell structures. Invading T lymphocytes have been reported to exhibit such internally high expression levels, with only individuated exterior cells expressing high levels of uPARs (Bianchi et al. 1996). A biological spatio-temporal model of tumour invasion reported high levels of uPA of the tumour's leading edge but also found extremely high levels on the invading mass' interior (Adam et al. 2001).

The y-waves occur within the 2D-spatial model also (Figs. 2, 3), where one may observe graduated levels of binding for c. One can observe that the largest concentration of c begins and remains at the epicentre of the population.

All results show a significant correlative relationship between the ECM levels, $v(t, x)$, and the destructive molecular species, $m_{f,1}(t, x)$, and therefore a wave of ECM destruction follows closely behind the travelling wave of the cancer cell population. This is an indicator of the indirect relationship between the cancer growth mechanism and the cancer population itself (i.e., acting through the intermediate degradative protein species $m_{f,1}$).

Results generated using a heterogeneous initial ECM density (Figs. 4, 5, 6) varied from the previously observed results with similar behaviour, nonetheless. One observes the spiking behaviours developing into a particularly defined wave front for the growing cancer population. Here, the boundary wave-like solution may be caused by the high affinity between the cancer cell population and the ECM.

Although it is difficult to depict this behaviour, one again observes y-waves in the numerics for the behaviour at the interior of the cancer population. This is masked by the isosurface for the spiking shell of the cancer population. The y-waves play an important role in determining the initial behaviour of the cancer population, during growth and establishment of the perimeter. It is unclear whether these waves contribute to the dramatic change in behaviour and form $t \in (9, 15)$.

Just as in the 1D- and 2D-spatial homogeneous ECM cases, one can observe the initial spatial splitting of the cancer population. Unlike in the homogeneous case (Figs. 2, 3), however, the heterogeneity appears to mediate the consolidation of the cancer subpopulations (Figs. 4b, 5b) into the characteristic tumour that one associates with the biological paradigm.

Given that a periodic function is used to generate the ECM heterogeneity, it is not terribly surprising that the result produced ($t \leq 20$) resembles that of a cyclic environment, with 180° turn symmetry. Further results (not shown) were generated with an asymmetric, or with non-radial symmetry with respect to the initial positioning of the tumour. These results again displayed an asymmetric splitting of the population (typically into two spatially distinct subpopulations) with the larger portion of the subpopulation migrating to those regions with the steepest ECM gradients. Given that all of these environments were normalised with respect to their overall nutritional capacity, the underlying ECM patterning has no significant bearing on the invasive success of the tumour.

Moreover, the cancer, in this 2D-spatial 1D-structural heterogeneous case, is particularly exploitative of its environment, protruding into areas of low ECM density before the diffusion of the molecular species through the more dense sections of the ECM allows the remainder of the population to follow. This feature of the cancer behaviour is repeated until total permeation of the spatial domain occurs. This also leads to the boundary of the cancer population becoming somewhat amorphous, as one observes with cancer in the natural, biological environment of the human tissue. It may be interesting to consider the case in which molecular species are more free to diffuse into areas of lower ECM density.

5.2 uPA in the Presence of Inhibitor PAI-1: 2D-Spatial 2D-Structural Results

Results generated using a heterogeneous initial ECM density were similar to those generated for the system with 1-structural dimension (in the absence of PAI-1, Figs. 7, 8, 9). One observes again that the spiking behaviours developing into a particularly defined wave front for the growing cancer population. Again, this is likely to be due to the attractive forces, leading to haptotaxis, between the cellular population and the ECM, causing cells to chemotactically self-aggregate on the boundary of the tumour. This is also likely accentuated by the local inhibition of invasion (through PAI-1 binding), which contrasts the advancement of the tumour boundary and encourages hyper-localised behaviours.

All of those significant features, appearing in the case of 1D-structural dimension (in the absence of PAI-1), appear in those for 2-structural dimensions (in the presence of PAI-1), with the important difference being that the nature of the tumour in this 2D-structural case develops at a much slower rate. This is expected behaviour given that the introduction of a 2nd structural dimension, in this case, corresponds to the introduction of an inhibitor to the degradative activation protein, uPA. The apparent rate of change in tumour growth can be approximately given by $\alpha_{m_{f,1}} - \gamma_{m_{f,1}}$ such that the rate by which the tumour is slowed down is equal to the binding ability of the inhibitor. This can be clearly seen in the differences in morphology at $t < 20$ (Figs. 7, 8).

6 Discussion and Conclusions

In the case where we consider a homogeneous cancer population and ECM density (Figs. 2, 3), one observes a logistic boundary that expands, unimpeded, to its maximal

radius within the given domain. Within this one observes a lower peak that clearly continues to expand throughout the space with the y-wave behaviour (which can be observed within the raw data), although at much lower values for C. This is likely due to the initial conditions remaining constant with the addition of a spatial dimension, causing values for c to be distributed and for C to be reduced. Overall, these solutions were in line with the 1D-spatial test-systems but not indicative of natural cancer behaviour.

Once we endow the cancer species with its natural habitat (the heterogeneous ECM), one observes behaviours absolutely characteristic of the biological system. These behaviours included the volume filling properties for the inside of the tumour, the aggressive behaviour of the cancer's perimeter, and the primary invasion into areas of lower tissue density. It is not clear whether or not the initial splitting of the cancer into two subpopulations is characteristic of nature but certainly is of the model, which is again likely a consequence of the initial conditions.

It can also be directly observed that the numerical solution is stable in its spatial dynamics but unstable in structural dynamics, which can be seen from the total permeation of $\mathcal{P}$ on the boundary of c whilst the spatially considered cancer population, C, does not exhibit uncontrolled migration in $\mathcal{D}$. The areas of higher values for C (Fig. 6) can be attributed to the fact that y-waves continue to exist within the body of the tumour and behave as in the 1D-spatial model.

The largest errors arise from the structural differentiation in the second term of the equation for $\frac{\partial c}{\partial t}$, where we incur second-order errors as a result of the symmetric difference quotient approximation. This method is commonly used, and there are no clear contenders to be used in its place since reaching a higher-order approximation is far more difficult than incurring computational and processing penalties as a result of increasing the number of required arithmetic calculations.

We then have a third-order error that results from the trapezoidal approximation on the local integral. This could, potentially, be improved by, for example, taking a higher-order approximation, such as Simpson's rule polynomial approximation, but one necessarily has a trade-off between accuracy and computational intensity.

On the whole, these errors tend to be small so long as δ_x and δ_y are kept sufficiently small, $\delta_x, \delta_y \leq 10^{-2}$.

The result of stability analysis was to confirm the conclusions of the numerical simulations that, notwithstanding ones ability to compensate for the errors produced, the system is unstable in y. Any perturbation induced with nonzero y-component will result in the exponential growth of the perturbation through the structure space.

This simply implies that for fine perturbations in x, one must have sufficiently low migration in y so as to allow the profile to remain stable. This is particularly interesting when taken in combination with the numerical solutions which revealed explosive instabilities upon rapid migration to the y boundary, or the boundary of $\bar{\mathcal{P}}$, $\partial \bar{\mathcal{P}}$.

Given that, for stability, one considers the magnitude (or absolute values) of the parameters involved, one has that **m** is unstable under all conditions and for small perturbation around any hypothetical stable solution. We also find that v is stable at the cancer-ECM equilibrium such that, since we are interested in the cancer growth and destruction of its local environment, the system is stable, notwithstanding the instability in **m**.

Numerical results show interesting behaviours, particularly with the introduction of y-waves, resulting from the structural considerations in c. One sees the expected characteristics of the aggressive cancer species considered, with smooth degradation of the ECM and concurrent advancement of the cancer species to encroach on the healthy tissue. One shows how various considerations as to how one could amend the system result in more reasonable and expected behaviours in the cancer species but how, ultimately, the results that most closely correlate with the biological paradigm require a rethink of the underlying assumptions for the system, as a whole.

The numerical results for the system may elucidate an interesting propensity of the biological cancer system to utilise unconventional mechanisms of invasion, under the influence of chemical inhibitors. Inhibiting the uPA system appears, in some way, to impede the uniform invasion of the stroma by this aggressive cancer species, whilst allowing the ECM to remain intact by reducing the cancer's ability to degrade collagen has allowed the cancer to more readily utilise haptotactic behaviours. Therefore, what one observes in the inhibitor system, in comparison with its counterpart, is a more sporadic distribution of cancer cells who invade but do not degrade the ECM (growing in areas where competition for space is reduced).

This gives rise to important biological questions about how one treats and prevents the spread of these cells, since inhibition may cause greater clinical issues. The inhibitors fail to inhibit the initial devastation of the ECM by uPA but leave the ECM open to exploitation. This may be a survival mechanism utilised by cancer and may have been evolutionarily beneficial to it propensity to arise in the human body, rather than acting to the detriment of its progression.

A Parameter Set

c	:	$D_c = 10^{-4}$	$\xi_v = 5 \times 10^{-2}$	$\xi_1 = 1 \times 10^{-3}$	$\mu_c = 0.1$
		$S_{cc} = 10^{-4}$	$S_{cv} = 10^{-4}$	$\mathfrak{v}_c = 0.524$	$\mathfrak{v}_v = 0.476$
i-state	:		$\varepsilon = 0.1$	$\beta = 0.5$	$\gamma_y = 0$
v	:		$\gamma_v = 10$	$\mu_v = 0.05$	
$m_{b,1}$	:	$D_{m_{b,1}} = 10^{-3}$	$\alpha_{m_{b,1}} = 0.1$	$\gamma_{m_{b,1}} = 0.1$	
$m_{b,1}$	:	$D_{m_{b,1}} = 10^{-3}$	$\alpha_{m_{b,1}} = 0.1$	$\gamma_{m_{b,2}} = 0.1$	
$m_{f,1}$	:	$D_{m_{f,1}} = 10^{-3}$	$\alpha_{m_{f,1}} = 0.5$	$\gamma_{m_{f,1}} = 0.1$	

References

Adam J, Bellomo N (1996) A survey of models for tumor-immune system dynamics. Birkhäuser, Boston

Adam L, Mazumdar A, Sharma T, Jones TR, Kumar R (2001) A three-dimensional and temporo-spatial model to study invasiveness of cancer cells by heregulin and prostaglandin e_2. Cancer Res 61:81–87

Allen EJ (2009) Derivation of stochastic partial differential equations for size- and age-structured populations. J Biol Dyn 3(1):73–86. https://doi.org/10.1080/17513750802162754

Al-Omari J, Gourley S (2002) Monotone travelling fronts in an age-structured reaction-diffusion model of a single species. J Math Biol 45(4):294–312. https://doi.org/10.1007/s002850200159

Andasari V, Gerisch A, Lolas G, South AP, Chaplain MAJ (2011) Mathematical modeling of cancer cell invasion of tissue: biological insight from mathematical analysis and computational simulation. J Math Biol 63(1):141–171. https://doi.org/10.1007/s00285-010-0369-1

Anderson A, Chaplain MAJ (1998) Continuous and discrete mathematical models of tumor-induced angiogenesis. Bull Math Biol 60(5):857–899

Anderson ARA, Chaplain MAJ, Newman EL et al (2000) Mathematical modelling of tumour invasion and metastasis. J Theor Med 2(2):129–154

Ayati BP (2006) A structured-population model of proteus mirabilis swarm-colony development. J Math Biol 52(1):93–114. https://doi.org/10.1007/s00285-005-0345-3

Barinka C, Parry G, Callahan J et al (2006) Structural basis of interaction between urokinase-type plasminogen activator and its receptor. J Mol Biol 363(2):482–495

Basse B, Ubezio P (2007) A generalised age- and phase-structured model of human tumour cell populations both unperturbed and exposed to a range of cancer therapies. Bull Math Biol 69(5):1673–1690

Bellomo N, Preziosi L (2000) Modelling and mathematical problems related to tumor evolution and its interaction with the immune system. Math Comput Model 32:413–452

Bellomo N, Li NK, Maini PK (2008) On the foundations of cancer modelling: selected topics, speculations, and perspectives. Math Models Methods Appl Sci 18(4):593–646

Benzekry S, Lamont C, Beheshti A et al (2014) Classical mathematical models for description and prediction of experimental tumor growth. PLoS Comput Biol 10(8):e1003,800

Bertuzzi A, D'Onofrio A, Fasano A, Gandolfi A (2004) Modelling cell populations with spatial structure: steady state and treatment-induced evolution of tumour cords. Discrete Contin Dyn Syst Ser B 4(1):161–186

Bhuvarahamurthy V, Schroeder J, Kristiansen G et al (2005) Differential gene expression of urokinase-type plasminogen activator and its receptor in human renal cell carcinoma. Oncol Rep 14(3):777–782

Bianchi E, Ferrero E, Fazioli F, Mangili F, Wang J, Bender JR, Blasi F, Pardi R (1996) Integrin-dependent induction of functional urokinase receptors in primary t lymphocytes. J Clin Investig 98(5):1133–1141

Binder BR, Mihaly J, Prager GW (2007) uPAR–uPA–uPAI-1 interactions and signalling: a vascular biologist's view. Int J Vasc Biol Med 97:336–342

Busenberg S, Iannelli M (1983) A class of nonlinear diffusion problems in age-dependent population dynamics. Nonlinear Anal Theory Methods Appl 7(5):501–529. https://doi.org/10.1016/0362-546X(83)90041-X

Calsina À, Saldaña J (1995) A model of physiologically structured population dynamics with a nonlinear individual growth rate. J Math Biol 33(4):335–364. https://doi.org/10.1007/BF00176377

Chaplain MAJ, Lolas G (2005) Mathematical modelling of cancer cell invasion of tissue: the role of the urokinase plasminogen activation system. Math. Models Methods Appl Sci 11(2005):1685–1734

Chaplain MAJ, Ganesh M, Graham IG (2001) Spatio-temporal pattern formation on spherical surfaces: numerical simulation and application to solid tumour growth. J Math Biol 42(5):387–423

Chapman SJ, Plank MJ, James A, Basse B (2007) A nonlinear model of age and size-structured populations with applications to cell cycles. ANZIAM J 49(02):151

Chapman A, del Ama LF, Ferguson J, Kamarashev J, Wellbrock C, Huristone A (2014) Heterogeneous tumour subpopulations cooperate to drive invasion. Cell Rep 8:688–695

Chaurasia P, Aguirre-Ghiso JA, Liang OD et al (2006) A region in Urokinase plasminogen receptor domain III controlling a functional association with 5beta1 integrin and tumor growth. J Biol Chem 281(21):14852–14863

Clayton D, Schifflers E (1987) Models for temporal variation in cancer rates. I: age-period and age-cohort models. Stat Med 6(4):449–467

Cushing JM (1998) An introduction to structured population dynamics. In: CBMS-NSF regional conference series in applied mathematics, vol 71. SIAM . https://doi.org/10.1137/1.9781611970005.ch2

Cusulin C, Iannelli M, Marinoschi G (2005) Age-structured diffusion in a multi-layer environment. Nonlinear analysis: real world applications 6(1):207–223. https://doi.org/10.1016/j.nonrwa.2004.08.006

Danø K, Andreasen P, Grøndahl-Hansen J et al (1985) Plasminogen activators, tissue degradation, and cancer. Adv Cancer Res 44:139–266

Danø K, Rømer J, Nielsen BS, Bjørn S et al (1999) Cancer invasion and tissue remodeling-cooperation of protease systems and cell types. APMIS 107(1–6):120–127

de Roos AM (1997) A gentle introduction to physiologically structured population models. In: Tuljapurkar S, Caswell H (eds) Structured-population models in marine, terrestrial, and freshwater systems, popu-

lation and community biology series, vol 18. Springer, US, pp 119–204. https://doi.org/10.1007/978-1-4615-5973-3_5

Delgado M, Molina-Becerra M, Suárez A (2006) A nonlinear age-dependent model with spatial diffusion. J Math Anal Appl 313(1):366–380. https://doi.org/10.1016/j.jmaa.2005.09.042

Delitala M, Lorenzi T (2012) Asymptotic dynamics in continuous structured populations with mutations, competition and mutualism. J Math Anal Appl 389:439–451. https://doi.org/10.1016/j.jmaa.2011.11.076

Delitala M, Lorenzi T, Melensi M (2015) Competition between cancer cells and t cells under immunotherapy: a structured population approach. In: ITM web of conferences, vol 5. https://doi.org/10.1051/itmconf/20150500005

Deng Q, Hallam TG (2006) An age structured population model in a spatially heterogeneous environment: existence and uniqueness theory. Nonlinear Anal Theory Methods Appl 65(2):379–394. https://doi.org/10.1016/j.na.2005.06.019

Di Blasio G (1979) Non-linear age-dependent population diffusion. J Math Biol 8(3):265–284. https://doi.org/10.1007/BF00276312

Diekmann O, Temme NM (eds.) (1982) Nonlinear diffusion problems. No. 28 in MC syllabus. Mathematisch Centrum, Amsterdam

Diekmann O, Metz JAJ (1994) On the reciprocal relationship between life histories and population dynamics. In: Lecture notes in biomathematics, Chapter Frontiers in mathematical biology, vol 100. Springer, Berlin, pp 263–279

Diekmann O, Heijmans HJAM, Thieme HR (1984) On the stability of the cell size distribution. J Math Biol 19(2):227–248

Diekmann O, Gyllenberg M, Metz JAJ, Thieme H (1992) The 'cumulative' formulation of (physiologically) structured population models. CWI, Amsterdam

Domschke P, Trucu D, Gerisch A et al (2014) Mathematical modelling of cancer invasion: implications of cell adhesion variability for tumour infiltrative growth patterns. J Theor Biol 361:41–60

Domschke P, Trucu D, Gerisch A et al (2017) Structured models of cell migration incorporating molecular binding processes. J Math Biol 75:1517–1561. https://doi.org/10.1007/s00285-017-1120-y

Dufau I, Frongia C, Sicard F, Dedieu L et al (2012) Multicellular tumor spheroid model to evaluate spatio-temporal dynamics effect of chemotherapeutics: application to the gemcitabine/CHK1 inhibitor combination in pancreatic cancer. BMC Cancer 12(1):15

Duffy MJ, Maguire TM, McDermott EW et al (1999) Urokinase plasminogen activator: a prognostic marker in multiple types of cancer. J Surg Oncol 71(2):130–135

Dyson J, Webb G (2000a) A nonlinear age and maturity structured model of population dynamics i. Basic theory. J Math Anal Appl 242:93–104

Dyson J, Webb G (2000b) A nonlinear age and maturity structured model of population dynamics ii. Chaos. J Math Anal Appl 242:255–270

Ellis V, Danø K (1993) Potentiation of plasminogen activation by an anti-urokinase monoclonal antibody due to ternary complex formation. A mechanistic model for receptor-mediated plasminogen activation. J Biol Chem 268(7):4806–13

Fitzgibbon W, Parrott M, Webb G (1995) Diffusion epidemic models with incubation and crisscross dynamics. Math Biosci 128(1–2):131–155. https://doi.org/10.1016/0025-5564(94)00070-G

Galle J, Hoffmann M, Aust G (2009) From single cells to tissue architecture—a bottom-up approach to modelling the spatio-temporal organisation of complex multi-cellular systems. J Math Biol 58(1–2):261–283

Garroni MG, Langlais M (1982) Age-dependent population diffusion with external constraint. J Math Biol 14(1):77–94. https://doi.org/10.1007/BF02154754

Gatenby RA, Gawlinski ET (1996) A reaction–diffusion model of cancer invasion. Cancer Res 56(24):5745–5753

Gerisch A, Chaplain M (2008) Mathematical modelling of cancer cell invasion of tissue: local and non-local models and the effect of adhesion. J Theor Biol 250(4):684–704

Godár S, Hořejší V, Weidle UH et al (1999) M6P/IGFII-receptor complexes urokinase receptor and plasminogen for activation of transforming growth factor-β1. Eur J Immunol 29(3):1004–1013

Gurtin M, MacCamy R (1981) Diffusion models for age-structured populations. Math Biosci 54(1–2):49–59. https://doi.org/10.1016/0025-5564(81)90075-4

Gyilenberg M, Webb GF (1990) A nonlinear structured population model of tumor growth with quiescence. J Math Biol 28:671–694

Gyllenberg M (1982) Nonlinear age-dependent population dynamics in continuously propagated bacterial cultures. Math Biosci 62(1):45–74. https://doi.org/10.1016/0025-5564(82)90062-1

Gyllenberg M (1986) The size and scar distributions of the yeast saccharomyces cerevisiae. J Math Biol 24(1):81–101. https://doi.org/10.1007/BF00275722

Gyllenberg M, Webb G (1987) Age-size structure in populations with quiescence. Math Biosci 86(1):67–95. https://doi.org/10.1016/0025-5564(87)90064-2

Hanahan D, Weinberg RA (2011) The hallmarks of cancer: the next generation. Cell 144:646–674

Hsieh YH (1991) Altruistic population model with sex differences. In: Arnino O, Axelrod DE, Kimmel M (eds) Mathematical population dynamics. Lecture notes in pure and applied mathematics, vol 131. Marcel Dekker Inc, New York

Huai Q, Mazar AP, Kuo A, Parry GC et al (2006) Structure of human urokinase plasminogen activator in complex with its receptor. Science (New York, N.Y.) 311(5761):656–659

Huang C (1994) An age-dependent population model with nonlinear diffusion in $\mathbf{R}^n$. Q Appl Math 52:377–398

Huyer W (1994) A size-structured population-model with dispersion. J Math Anal Appl 181(3):716–754. https://doi.org/10.1006/jmaa.1994.1054

Khanna M, Wang F, Jo I et al (2011) Targeting multiple conformations leads to small molecule inhibitors of the uPAR·uPA protein-protein interaction that block cancer cell invasion. ACS Chem Biol 9(11):1232–1243. https://doi.org/10.1021/cb200180m

Kimmel M, Darzynkiewicz Z, Arino O, Traganos F (1984) Analysis of a cell cycle model based on unequal division of metabolic constituents to daughter cells during cytokinesis. J Theor Biol 110:637–664

Kondraganti S, Gondi CS, McCutcheon I et al (2006) RNAi-mediated downregulation of urokinase plasminogen activator and its receptor in human meningioma cells inhibits tumor invasion and growth. Int J Oncol 28(6):1353–1360

Kunisch K, Schappacher W, Webb G (1985) Nonlinear age-dependent population dynamics with random diffusion. Comput Math Appl 11(1–3):155–173

Langlais M (1988) Large time behavior in a nonlinear age-dependent population dynamics problem with spatial diffusion. J Math Biol 26(3):319–346. https://doi.org/10.1007/BF00277394

Langlais M, Milner FA (2003) Existence and uniqueness of solutions for a diffusion model of host-parasite dynamics. J Math Anal Appl 279(2):463–474. https://doi.org/10.1016/S0022-247X(03)00020-9

Leksa V, Godar S, Cebecauer M et al (2002) The N terminus of mannose 6-phosphate/insulin-like growth factor 2 receptor in regulation of fibrinolysis and cell migration. J Biol Chem 277(43):40575–40582

Li Y, Cozzi P (2007) Targeting uPA/uPAR in prostate cancer. Cancer Treat Rev 33(6):521–527

Liang X, Yang X, Tang Y et al (2008) RNAi-mediated downregulation of urokinase plasminogen activator receptor inhibits proliferation, adhesion, migration and invasion in oral cancer cells. Oral Oncol 44(12):1172–1180

Liu D, Ghiso JA, Estrada Y et al (2002) EGFR is a transducer of the urokinase receptor initiated signal that is required for in vivo growth of a human carcinoma. Cancer Cell 1(5):445–457

Lorz A, Lorenzi T, Hochberg ME, Clairambault J, Perthame B (2013) Populational adaptive evolution, chemotherapeutic resistance and multiple anti-cancer therapies. ESAIM Math Model Numer Anal 47:377–399. https://doi.org/10.1051/m2an/2012031

MacCamy R (1981) A population model with nonlinear diffusion. J Differ Equ 39(1):52–72. https://doi.org/10.1016/0022-0396(81)90083-8

Madsen DH, Engelholm LH, Ingvarsen S et al (2007) Extracellular collagenases and the endocytic receptor, urokinase plasminogen activator receptor-associated protein/Endo180, cooperate in fibroblast-mediated collagen degradation. J Biol Chem 282(37):27037–27045

Magal P, Ruan S (eds) (2008) Structured population models in biology and epidemiology. Springer, Berlin

Meinzer H, Sandblad B (1985) A simulation model for studies of intestine cell dynamics. Comput Methods Progr Biomed 21(2):89–98

Metz JAJ, Diekmann O (1986) A gentle introduction to structured population models: three worked examples. In: Lecture notes in biomathematics, vol 68, chap. The dynamics of physiologically structured populations, pp 3–45. Springer, Berlin

Murray JD, Oster GF (1984) Cell traction models for generating pattern and form in morphogenesis. J Math Biol 19(3):265–279

Peng PL, Hsieh YS, Wang CJ et al (2006) Inhibitory effect of berberine on the invasion of human lung cancer cells via decreased productions of urokinase-plasminogen activator and matrix metalloproteinase-2. Toxicol Appl Pharmacol 214(1):8–15

Peng L, Trucu D, Lin P et al (2017) A multiscale mathematical model of tumour invasive growth. Bull Math Biol 79:389–429. https://doi.org/10.1007/s11538-016-0237-2

Persson M, Madsen J, Østergaard S et al (2012) 68Ga-labeling and in vivo evaluation of a uPAR binding DOTA- and NODAGA-conjugated peptide for PET imaging of invasive cancers. Nucl Med Biol 39(4):560–569

Perthame B (2007) Transport equations in biology. Birkhauser Verlag, Basel

Prigogine I, Lefever R (1980) Stability problems in cancer growth and nucleation. Comp Biochem Physiol Part B Comp Biochem 67(3):389–393

Rhandi A (1998) Positivity and stability for a population equation with diffusion on l^1. Positivity 2(2):101–113. https://doi.org/10.1023/A:1009721915101

Rijken DC (1995) 2 Plasminogen activators and plasminogen activator inhibitors: biochemical aspects. Bailliere's Clin Haematol 8(2):291–312

Sinko JW, Streifer W (1967) A new model for age-size structure of a population. Ecology 48(6):910–918. https://doi.org/10.2307/1934533

Smith HW, Marshall CJ (2010) Regulation of cell signalling by uPAR. Nat Rev Mol Cell Biol 11(1):23–36

So JWH, Wu J, Zou X (2001) A reaction–diffusion model for a single species with age structure. I travelling wavefronts on unbounded domains. Proc R Soc Lond Ser A Math Phys Eng Sci 457(2012):1841–1853. https://doi.org/10.1098/rspa.2001.0789

Stillfried GE, Saunders DN, Ranson M et al (2007) Plasminogen binding and activation at the breast cancer cell surface: the integral role of urokinase activity. Breast Cancer Res 9(1):R14

Sugioka K, Kodama A, Okada K et al (2013) TGF-β2 promotes RPE cell invasion into a collagen gel by mediating urokinase-type plasminogen activator (uPA) expression. Exp Eye Res 115:13–21

Trucco E (1965a) Mathematical models for cellular systems the von foerster equation. Part i. Bull Math Biophys 27(3):285–304. https://doi.org/10.1007/BF02478406

Trucco E (1965b) Mathematical models for cellular systems. The von foerster equation. Part ii. Bull Math Biophys 27(4):449–471. https://doi.org/10.1007/BF02476849

Trucu D, Lin P, Chaplain MAJ, Wang Y (2013) A multiscale moving boundary model arising in cancer invasion. Multiscale Model Simul 11(1):309–335

Trucu D, Domschke P, Gerisch A, Chaplain MAJ (2017) Multiscale computational modelling and analysis of cancer invasion. In: Springer lecture notes in mathematics, CIME foundation subseries, vol 2167, pp 275–310. Springer

Tucker SL, Zimmerman SO (1988) A nonlinear model of population dynamics containing an arbitrary number of continuous structure variables. SIAM J Appl Math 48(3):549–591. URL http://www.jstor.org/stable/2101595

Waltz DA, Chapman HA (1994) Reversible cellular adhesion to vitronectin linked to urokinase receptor occupancy. J Biol Chem 269(20):14,746–50

Waltz DA, Natkin LR, Fujita RM et al (1997) Plasmin and plasminogen activator inhibitor type 1 promote cellular motility by regulating the interaction between the urokinase receptor and vitronectin. J Clin Investig 100(1):58–67

Wei Y, Waltz DA, Rao N et al (1994) Identification of the urokinase receptor as an adhesion receptor for vitronectin. J Biol Chem 269(51):32,380–8

Yamaguchi N, Mizutani T, Kawabata K, Haga H (2015) Leader cells regulate collective cell migration via rac activation in the downstream signaling of integrin β1 and pi3k. Sci Rep 5(7656):1–8